IEEE GRSS Brazil' Chapter

7th GRSS Young Professionals & ISPRS SC Summer School

IEEE/GRSS`Brazil Chapter

Chair

Carlos Grohmann
USP

Invited Researcher

Michael Steinmayer
SulSoft Sistemas

Young Professional

Julia Cucco Dalri
UDESC

November 11th, 2021 | 9:00h (-3 GMT)

Mathematical Morphology in Processing and Analysis of DEMs

B. S. Daya Sagar
Indian Statistical Institute

Supported by: fapesc, GRSS, isprs, ISPRS, IGVEC, Canoinhas

Organized by: UDESC, UNOCHAPECÓ

Co-Organized by: PUC RIO, INPE, UFMG, UFPR, unesp, UFMS, Unoeste

MATHEMATICAL MORPHOLOGY IN PROCESSING AND ANALYSES OF DIGITAL ELEVATION MODELS

B.S. Daya Sagar
http://www.isibang.ac.in/~bsdsagar
Systems Science and Informatics Unit (SSIU)
Indian Statistical Institute-Bangalore Centre
IEEE GRSS DISTINGUISHED LECTURER (2020-2022)
http://www.grss-ieee.org/education/distinguished-lecturers/

IEEE GRSS BRAZIL'S CHAPTER GRSS YOUNG PROFESSIONALS & ISPRS SC SUMMER SCHOOL
Thursday, November 11, 2021
17.30 (IST)
https://www.youtube.com/watch?v=52pLx6lfeIU

Science Out of DEMs

Spatial Data

What does it have?

Relevant Mathematics

Science out of spatial data and spatial information

- Digital Elevation Model (DEM) is an Engineering Marvel: An important source of data for geoscientists
- DEMs ($f(x,y)$)are with rich but hidden geometric, morphologic, and topologic (GMT) quantities (X) and the associated parameters.
- Having expertise in mathematical morphology and fractal geometry would be a huge advantage to unravel GMT quantities and associated parameters
- Studying DEMs, GMT quantities and associated parameters across space-time scales facilitate researchers derive important science-outcomes to develop models through which one can better understand the dynamical behaviors of several terrestrial phenomena and processes of the Earth planet and Earth-like extra-terrestrial planets

Geometric, Morphologic, and Topologic (GMT) quantities include peaks, pits, global and local minima and maxima, contours, crenulations, unique valley and ridge connectivity networks, topographic depressions, flat regions, mountain objects. Associated parameters include width function determination; roughness estimation; directional roughness estimation; structural and textural complexity; basin geodesics; basin-stage classification; feature mapping; quantitative characterization and reasoning; modelling, simulation and visualization

Why & What

To understand the dynamical behavior of surficial process, a good **spatiotemporal model** is essential. To develop such a model, well-**analyzed** and well-**reasoned information** that could be **retrieved** from spatial and/or temporal data are important required ingredients.

Mathematical Morphology is one of the better choices to deal with all these key aspects mentioned.

"Mathematical Morphology is an area of geoscience that most people don't realize will literally change the way they look at Earth!"

In Mathematical Morphology, Data **(*f(x,y)*)** is investigated with respect to another data (***B* or *g***, a probing rule with certain characteristic information) to address tasks such as retrieval, characterization, reasoning, modeling and simulation, and visualization.

This Lecture

- Digital Elevation Model (DEM) is an important source data for those who study Earth surface.
- Processing and analysis of the DEMs: Five cases studied with respect to
  - Skeletonization, SKIZ and WSKIZ
  - Granulometries
  - Geodesic spectrum
  - Morphological interpolations
  - Morphological distances

In One Slide

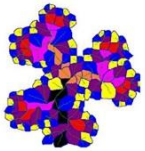

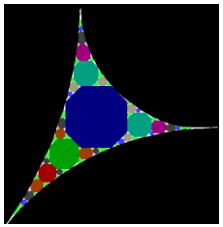

Multiscale opening/closing by rhombus

- Scale 1 , 40, 80, 120, 160

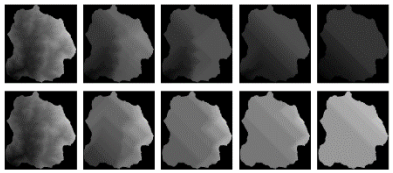

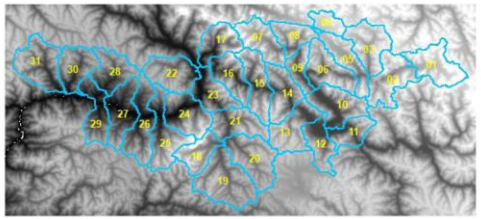

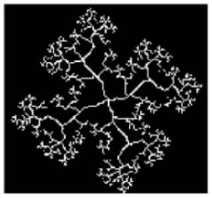

Fig. 2 Fluid FDN extracted from binary fractal basin.

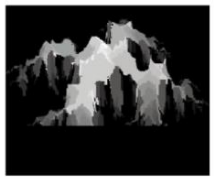

(a)

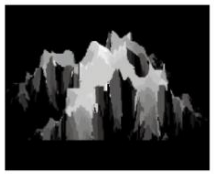

(b)

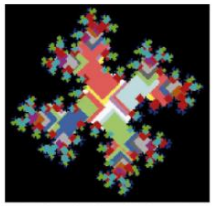

Fig. 3 A binary fractal basin after decomposition into TPRs.

Fig. 4 A fractal landscape generated from Fig. 3. Light and dark regions of DEM are visualized as high and low elevations, respectively (vertical exaggeration: (a) 5 and (b) 7).

and (9), producing a transcendental DEM (Fig. 3) from binary fractal (Fig. 1). The binary fractal

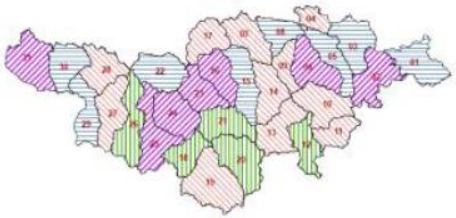

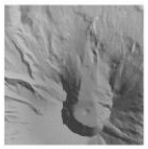

(a)

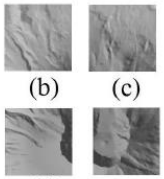

(b) (c) (d) (e)

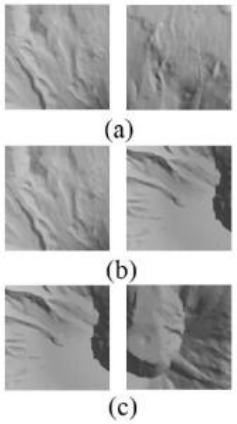

(a) (b) (c)

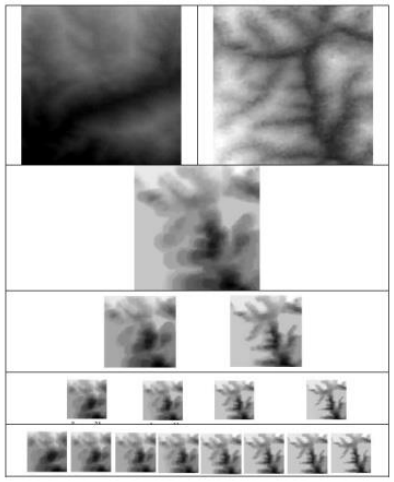

Overview

I. Digital Elevation Models (DEMs): An Important Source Data for Geoscientists

II. Mathematical Morphology: Notations, Equations, and Transformations

III. Mathematical Morphology in DEMs

- Skeletonization in DEMs and DEM Partitions
- Granulometries: Surficial roughness characterization/ quantification
- Geodesic Spectrum in Bottom Topography Studies
- Morphological Interpolations: Morphing of Source DEM into Target DEM
- Ranks for Pairs of Images; DEM Classification
- Morphological distances in spatial optimization and interaction modeling

IV. How the above studies could be integrated to better understand the surficial process dynamics?

B.S. DAYA SAGAR

Digital Elevation Models: An Important Source of Data for Geoscientists

Satellite technology has revolutionized the way we acquire terrestrial surface data. Such remotely sensed terrestrial data have made it possible to generate digital elevation models (DEMs) at multiple spatial and temporal scales by exploiting stereographic, interferometric, radargrammetric, and lidar principles [1]–[10]. Schemes adapted to generate DEMs are hugely successful, and, as such, DEM generation is considered an engineering marvel. In turn, the availability of DEMs to the geoscientific community is a blessing.

Both terrestrial and Earth-like planetary DEMs [e.g., Advanced Spaceborne Thermal Emission and Reflection Radiometer Global DEM, NASA DEM, Shuttle Radar Topography Mission (SRTM) DEM, Cartosat DEM, SPOT Stereo DEM, Chandrayaan DEM, Orbiter High Resolution Camera DEM, Mars DEM, Venus DEM, and lidar DEM] provide rich geometric, topologic, and morphologic information. As a result, DEMs offer an excellent resource for geoscientists, mathematicians, statisticians, geophysicists, computer scientists, cartographers, geographic information science professionals, engineers, and spatial planners in various phases of research to understand the spatiotemporal behavior of Earth and Earth-like planetary processes and visualize them in real time.

DEMs offer much more than is apparent at a visual inspection for those who are able to extract information of relevance to geometry, topology, and morphology from these models, which are available at multiple spatial and temporal scales. Until now, DEMs have been underutilized due to the lack of awareness of how they could be mathematically exploited, and they have not yet been studied for their geoscientific relevance. DEMs contain incredibly rich information that is best extracted with novel mathematical methods [11]–[26], such as discrete mathematics, geostatistics, exploratory data analysis, fractal geometry and scaling theory, fuzzy set theory, stochastic geometry, mathematical morphology, geomathematics, graph theory, compositional data analysis, nonlinear dynamical systems, and wavelets. It would serve the educational needs of the Society to encourage the training of experts in the relevance of DEMs in these areas. This would enrich the application of DEMs not only in geosciences but also in a host of other studies, such as resource estimation and identification, spatial planning, decision making, predictive analytics, and many more.

Processing and analysis of DEMs by these mathematical techniques would lead to sequentially intertwined outcomes, such as the application of these methods to unique valley–ridge connectivity networks, partitioned basins, surface roughness, geodesic spectra, categories of basins, ridge–valley spacing, geodesic distances, the rate of surficial evolution, synthetic terrestrial surfaces, revealing spatiotemporal behavior, and many more. Readers may refer to several technical papers for demonstrations on how these approaches are employed in the processing and analysis of DEMs as well as how challenges ranging from feature retrieval [27]–[37] to quantitative analysis and reasoning [38]–[52] and modeling and visualization [52]–[55] of the phenomenon- or process-specific spatiotemporal behavior are addressed.

Two illustrative examples, selected from numerous examples of our group, show the application of one of the previously mentioned mathematical theories on a synthetic random discrete topographic function [Figure 1(a)] and on a realistic DEM [Figure 2(b)] in mapping the unique connectivity networks [Figure 1(b)] and hierarchical watershed partitioning [Figure 1(c)] and the watershed-wise classification [Figure 2(b) and (c)] via directional roughness values computed through multivariate

Digital Object Identifier 10.1109/MGRS.2020.3031910
Date of current version: 16 December 2020

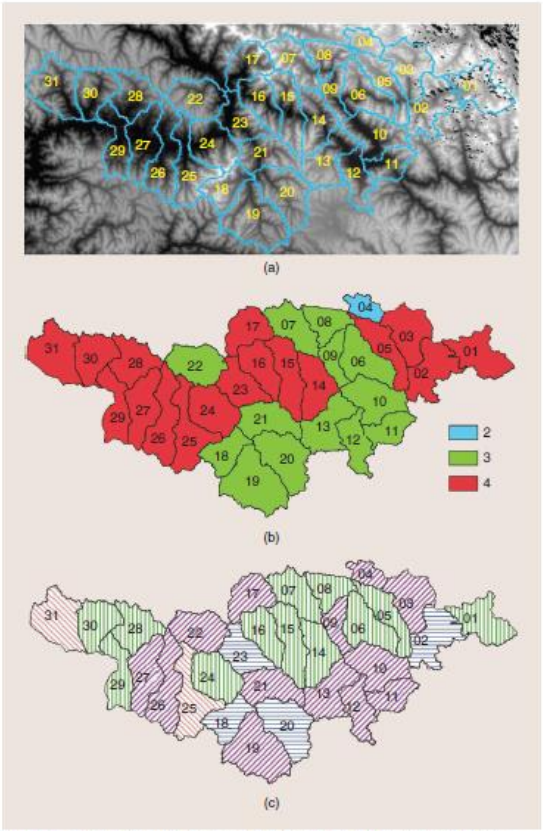

FIGURE 2. (a) An SRTM DEM of the lower Indus River subbasin, (b) a watershed-wise classification based on global roughness indexes computed using granulometric analysis, and (c) a watershed-wise classification of high-directional granulometric index values computed via directional granulometric analysis. For mathematical details, see [55].

geosciences, should be made mandatory, as should the necessary foundational mathematical courses required for these studies. This will both foster the self-reliance described previously and broaden the interdisciplinary nature of the field.

DEMs themselves are rich enough as a subject to warrant inclusion as a full-length subject at undergraduate and postgraduate levels, establishing a rigorous curriculum to train the next generation of geoscientists. This can be done by incorporating syllabi related to generating DEMs; characterizing their errors; devising descriptors via geometry, algebra, physics, and mathematics; developing physics-based algorithms for processing and analysis DEMs; and processing and analyzing DEMs using robust spatial algorithms. This dedicated, mathematically sound curriculum should be developed as a joint effort with mathematicians, statisticians, and scientists drawn from across disciplines: cartographers, computer engineers, photogrammetrists, and remote sensing specialists.

ACKNOWLEDGMENTS

Discussions via personal communications with Dr. Paul Rosen on the initial version and with Prof. Gabor Korvin on both versions helped improve the article significantly. The author is also grateful to the anonymous reviewers and the editor-in-chief, Prof. James Garrison, for their constructive criticism and many suggestions that helped strengthen this opinion piece.

AUTHOR INFORMATION

B.S. Daya Sagar (bsdsagar@isibang.ac.in) is a full professor at the Systems Science and Informatics Unit, Indian Statistical Institute, Bangalore Centre, India. His research interests include mathematical morphology; geographic information sciences; digital image processing; and fractals and multifractals and their applications in extraction, analyses, and modeling of geophysical patterns. He is an IEEE Geoscience and Remote Sensing Society (GRSS) Distinguished Lecturer for 2020–2022. He is a Senior Member of IEEE and the GRSS.

REFERENCES

[1] G. H. Rosenfield, "Stereo radar techniques," *Photogramm. Eng.*, vol. 34, no. 6, pp. 586–594, 1968.
[2] R. M. Goldstein and H. A. Zebker, "Two-dimensional phase unwrapping," *Radio Sci.*, vol. 23, no. 4, pp. 713–720, 1988. doi: 10.1029/RS023i004p00713.
[3] T. Toutin, "Generating DEM from stereo images with a photogrammetric approach: Examples with VIR and SAR data," *EARSel J. Adv. Remote Sens.*, vol. 4, no. 2, pp. 110–117, 1995.

Terrestrial and Earth-Like planetary DEMs

Synthetic DEMs
ASTER GDEM,
NASA DEM,
SRTM DEM,
Cartosat DEM,
SPOT Stereo DEM,
Chandrayaan DEM,
OHRC DEM,
Mars DEM,
Venus DEM,
LiDar DEM,
NEXTMap, and many more

Mathematical Morphology in DEMs

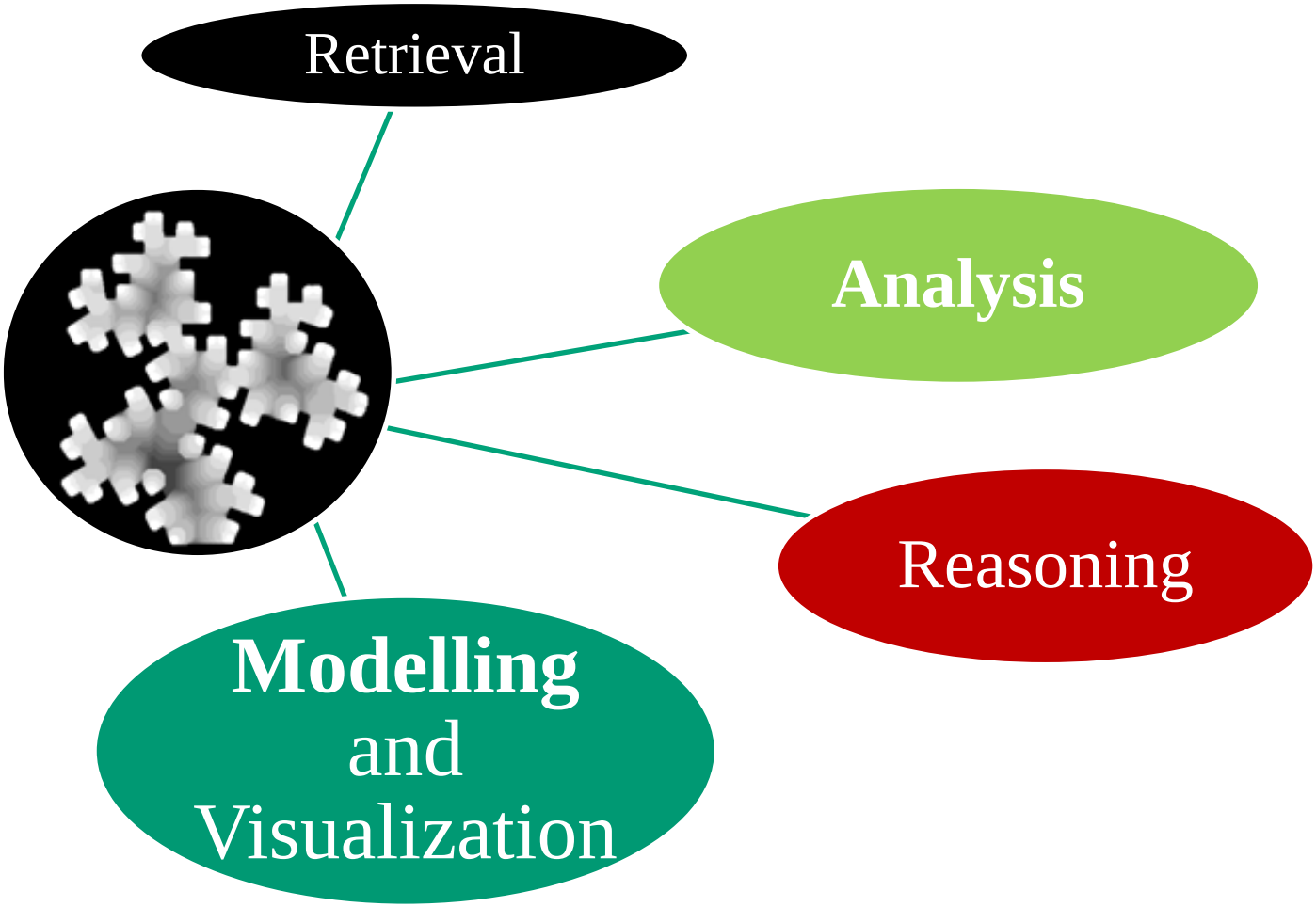

Digital Elevation Models

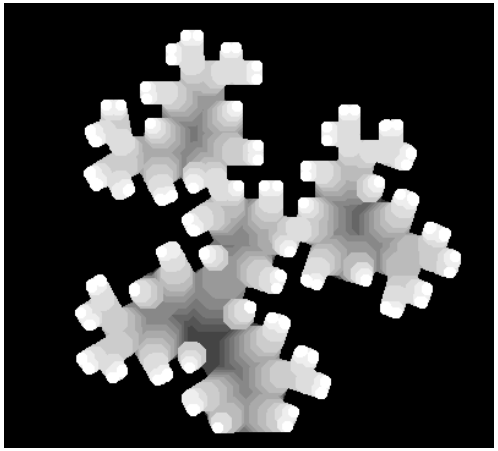

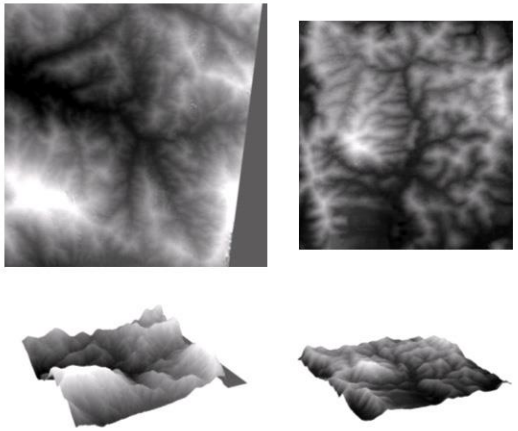

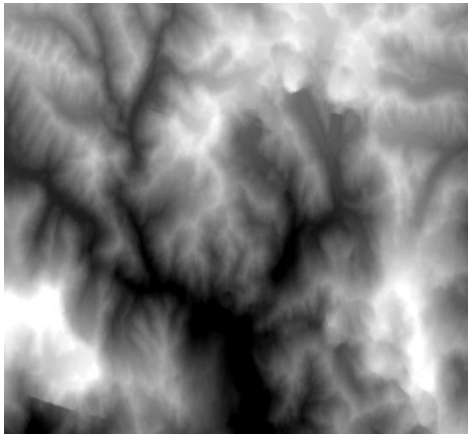

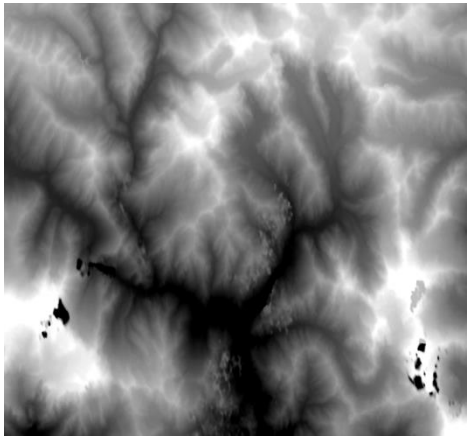

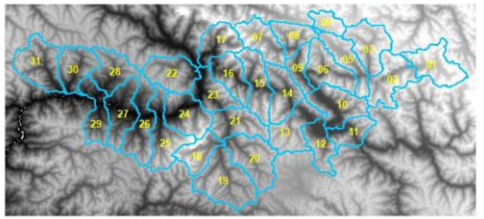

(c)

1.Fractal-Hortonian-DEM
2. TOPSAR DEMs
3. Cartosat-DEM
4. SRTM-DEM
5. Bathymetric SF-Bay
6. CartoSat DEM

Overview

I. Digital Elevation Models (DEMs): An Important Source Data for Geoscientists

II. Mathematical Morphology: Notations, Equations, and Transformations

III. Mathematical Morphology in DEMs

- Skeletonization in DEMs and DEM Partitions
- Granulometries: Surficial roughness characterization/ quantification
- Geodesic Spectrum in Bottom Topography Studies
- Morphological Interpolations: Morphing of Source DEM into Target DEM
- Ranks for Pairs of Images; DEM Classification
- Morphological distances in spatial optimization and interaction modeling

IV. How the above studies could be integrated to better understand the surficial process dynamics?

II. Mathematical Morphology

FOUNDING FATHERS OF

MATHEMATICAL MORPHOLOGY

Georges Matheron Jean Serra

Binary Mathematical Morphology

Grayscale Morphology

Graph Mathematical Morphology

Adaptive Mathematical Morphology

Basic Notations of Mathematical Morphology

Notation	
X, M, B	Spatial objects, Sets (e.g.: GMT Quantities)
$f(x,y)$	Spatial elevations over x and y spatial coordinates (e.g.: DEM or any other spatial function)
$A(f)$	Area of spatial function is sum of all the values over x,y
B and g	Flat structuring element and a non-flat structuring function
f^i and f^j	ith and jth spatial functions
$\oplus$, $\ominus$, $\bullet$, o	Symbols for dilation, erosion, closing and opening
$X^i \cap X^j$ and $X^i \cup X^j$	Intersection and Union of X^i and X^j
$f^i \wedge f^j$ and $f^i \vee f^j$	Infima and suprema of f^i and f^j
$X^i \cap X^j = X^i \cup X^j$	$X^i \equiv X^j$
$f^i \wedge f^j = f^i \vee f^j$	$f^i \equiv f^j$
$A(f^i) - A(f^j)$	Algebraic difference between the areas of f^i and f^j
$(f^i) - (f^j)$	Point-wise algebraic difference between f^i and f^j

Notations Contd…

Notation	
$d(X^i, X^j)$, $e(X^i, X^j)$, $\rho(X^i, X^j)$, $\sigma(X^i, X^j)$	Dilation, erosion, Hausdorff dilation and Hausdorff erosion distances between X^i and X^j
$A(f^i \wedge f^j)$ and $A(f^i \vee f^j)$	Areas of the infima and suprema of f^i and f^j
$d(f^i, f^j)$ and $e(f^i, f^j)$	Grayscale dilation and erosion distances between f^i and f^j
$(X \Theta B), (X \oplus B), (X \circ B), (X \bullet B)$	Morphological binary erosion, dilation, opening and closing of X with respect to B
$(X \Theta nB), (X \oplus nB), (X \circ nB), (X \bullet nB)$	Multiscale Morphological binary erosion, dilation, opening and closing of X w.r.t B
$(f \Theta B), (f \oplus B), (f \circ B), (f \bullet B)$	Morphological grayscale erosion, dilation, opening and closing of f with respect to B
$(f \Theta nB), (f \oplus nB), (f \circ nB), (f \bullet nB)$	Multiscale Morphological grayscale erosion, dilation, opening and closing of X w.r.t B
$B \oplus B \oplus B \oplus \ldots \oplus B = nB$	nth size B

Binary and Grayscale Morphological Equations

Operation	Equation
$(X \ominus B)$	$\{x: B_x \subseteq X\} = \cap X_{-b}$
$(X \oplus B)$	$\{x: (B_x \cap X) \neq \emptyset\} = \cup X_b$
$X \circ B$	$((X \ominus B) \oplus B))$
$(X \bullet B)$	$((X \oplus B) \ominus B))$
$(X \ominus nB)$	$(X \ominus B) \ominus B \ominus \ldots \ominus B$
$(X \oplus nB)$	$(X \oplus B) \oplus B \oplus \ldots \oplus B$
$(X \circ nB)$	$[(X \ominus nB) \oplus nB)]$
$(X \bullet nB)$	$[(X \oplus nB) \ominus nB)]$
$(X \circ nB) \bullet nB$	Alternative Sequential Filter Black
$(X \bullet nB) \circ nB$	Alternative Sequential Filter White

Operation	Equation
$(f \ominus B)\ (x,y)$	$min\{f(x+i, y+j), (i,j) \in B\}$
$(f \oplus B)\ (x,y)$	$max\{f(x+i, y+j), (i,j) \in B\}$
$(f \circ B)$	$((f \ominus B) \oplus B))$
$(f \bullet B)$	$((f \oplus B) \ominus B))$
$(f \ominus nB)$	$(f \ominus B) \ominus B \ominus \ldots \ominus B$
$(f \oplus nB)$	$(f \oplus B) \oplus B \oplus \ldots \oplus B$
$(f \circ nB)$	$[(f \ominus nB) \oplus nB)]$
$(f \bullet nB)$	$[(f \oplus nB) \ominus nB)]$
$(f \circ nB) \bullet nB$	Alternative Sequential Filter Black
$(f \bullet nB) \circ nB$	Alternative Sequential Filter White

Flat and Non-Flat Structuring Elements

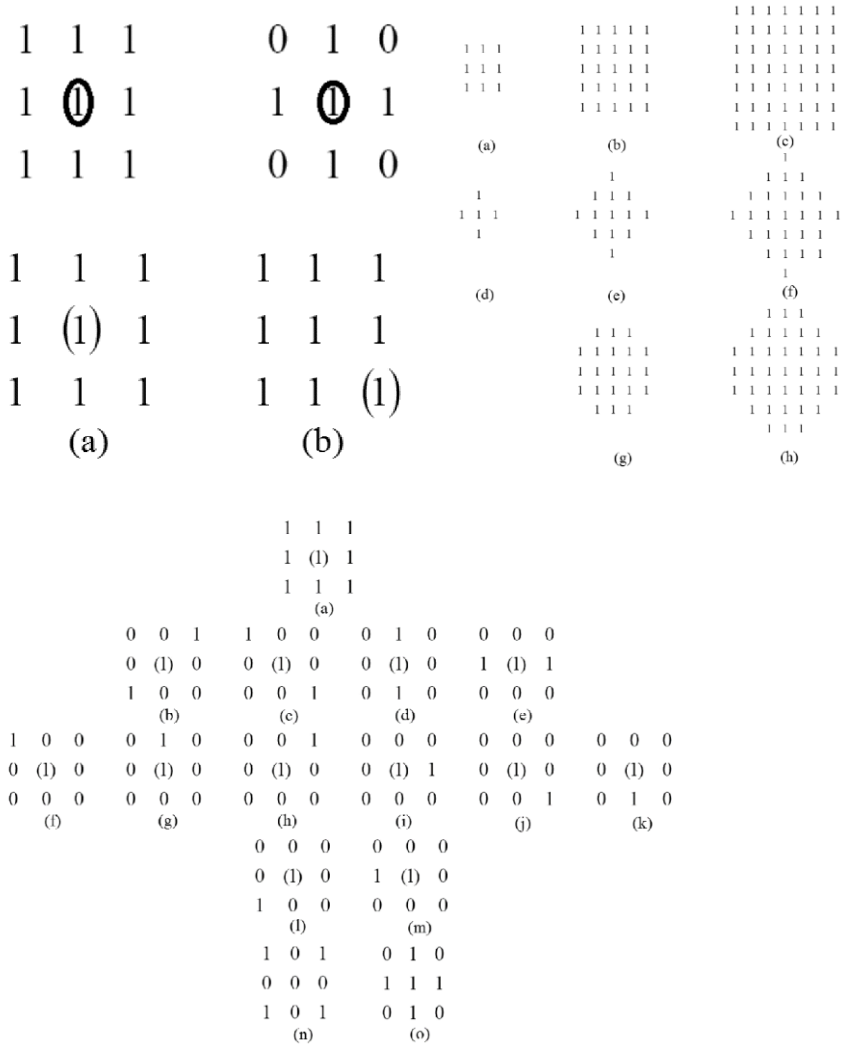

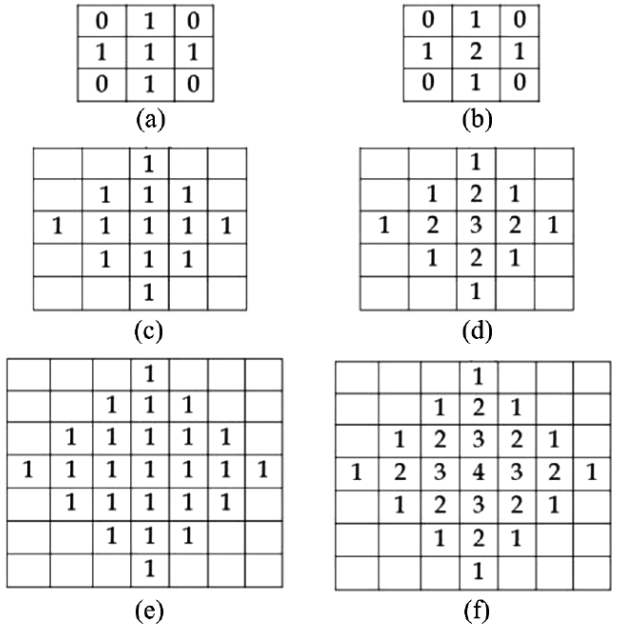

Fig. 2. (a) Rhombic symmetric flat-structuring element B of primitive size 3 × 3. (b) Rhombic symmetric nonflat-structuring element G of primitive size 3 × 3. (c) Flat rhombic B of size 5 × 5. (d) Nonflat rhombic G of size 5 × 5. (e) Flat rhombic B of size 7 × 7. (f) Nonflat rhombic G of size 7 × 7.

Grayscale Morphological Operations w.r.t Non-Flat Structuring Element (g)

$$(f \ominus g)(x,y) = \min_{(i,j)} \{ f(x+i, y+j) - g(i,j) \}$$

$$(f \oplus g)(x,y) = \max_{(i,j)} \{ f(x+i, y+j) + g(i,j) \}$$

$$\underbrace{g \oplus g \oplus \cdots \oplus g}_{n-times} = ng$$

$$(f \ominus ng) = ((f \ominus g) \ominus g \ominus \cdots \ominus g)$$

$$(f \oplus ng) = ((f \oplus g) \oplus g \oplus \cdots \oplus g)$$

Illustrations w.r.t. B and g

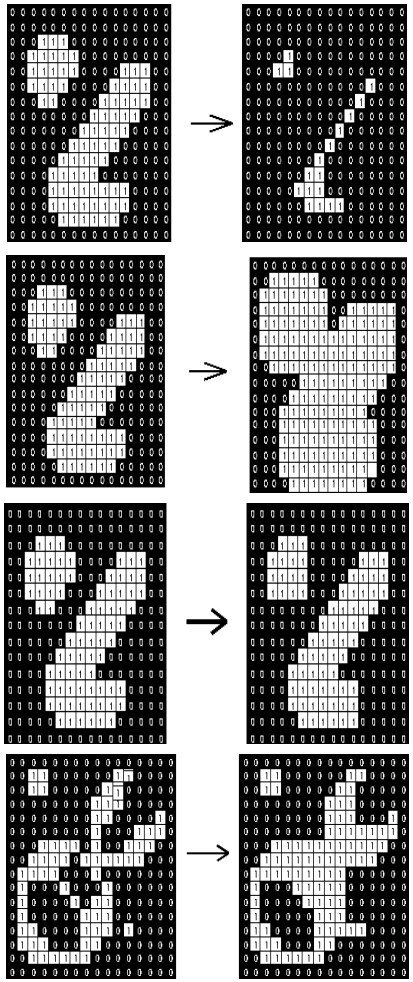

(a)

194	168	9
190	44	71
101	181	12

(b)

25	81	112
210	243	98
178	9	196

(a-b) Spatial fields.

(a)

194	194	168
194	190	71
190	181	181

(b)

168	9	9
44	44	9
101	12	12

(c)

196	195	169
195	194	181
191	190	182

(d)

44	8	7
43	9	8
44	11	10

Fig. 3. (a) Dilation of a spatial field shown in 1(a) by flat B of size 3x3, (b) Erosion of a spatial field shown in 1(a) by flat B of size 3x3, (c) Dilation of a spatial field shown in 1(a) by non-flat B of size 3x3, (d) Erosion of a spatial field shown in 1(a) by non-flat B of size 3x3.

Graph-Morphological Operations

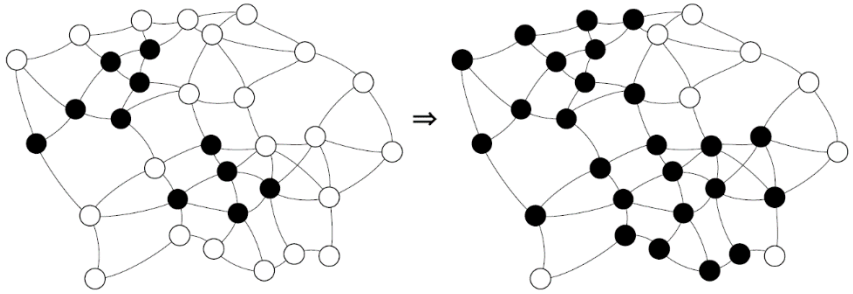

Figure 2: Non-structured elementary dilation of a binary graph.

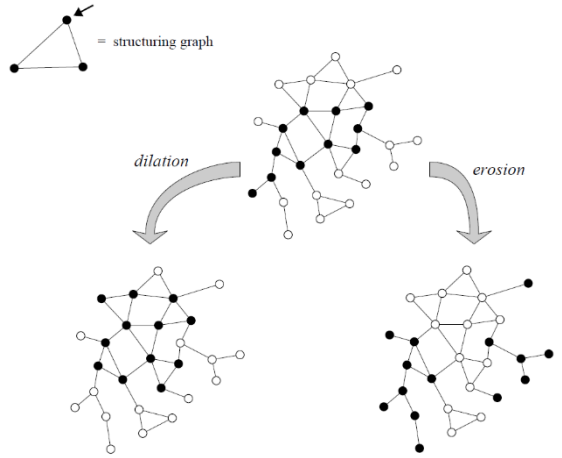

Figure 15: Dilation and erosion of a graph with respect to an s-graph.

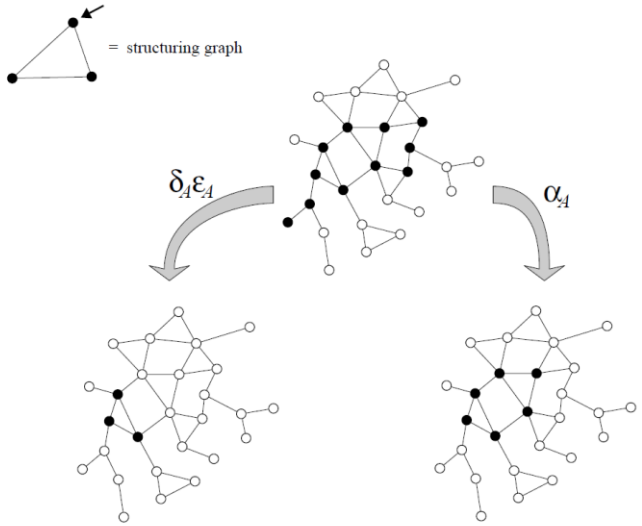

Figure 17: Two different openings of a binary graph with respect to a given s-graph.

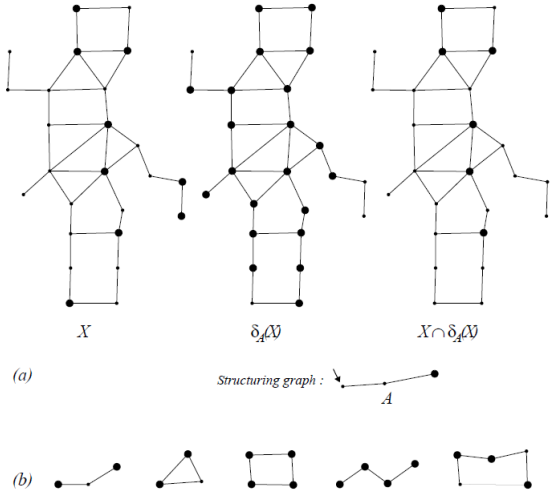

Figure 19: (a) Example of an annular opening. (b) Some typical invariants of the annular opening; note that every invariant is a "union of translates" of the invariant at the left.

Mathematical Morphological Operations

The mathematical morphological transformations useful to develop elegant algorithms to address the challenges in relation to Image Analysis and Spatial Informatics include:

- Morphological Erosion
- Morphological Dilation
- Morphological Opening
- Morphological Closing
- Multiscale Morphological Operations
- Hit-or-Miss Transformation
- Morphological Thinning , Thickening, Pruning
- Geodesic Morphological Operations
- Morphological Skeletonization
- Skeletonization by Zones of Influence
- Weighted Skeletonization by Zones of Influence
- Granulometries and Anti-Granulometries
- Morphological Distances
- Hausdorff Dilation Distances
- Hausdorff Erosion Distances
- Morphological Interpolations and Extrapolations
- The implementations of the aforementioned transformations in binary, grayscale, graph and geodesic domains

Binary Skeletonization, Granulometries, Morphological Interpolations, Morphological Distances

Operation	Equation
$SK(X)$	$\cup_{n=0}^{N} SK_n(X)$, where $SK_n(X) = (X \ominus nB) \backslash (X \ominus nB)\ o\ B$, for $n = 0, 1, 2, \ldots, N$
$H(X/B)$	$-\sum_{n=0}^{N} PnlnPn$ where
$d(X^i, X^j)$	$\min\{n: X^j \subseteq (X^i \oplus nB)\}$
$d(X^j, X^i)$	$\min\{n: X^i \subseteq (X^j \oplus nB)\}$
$e(X^i, X^j)$	$\min\{n: X^j \subseteq (X^i \ominus nB)\}$
$e(X^j, X^i)$	$\min\{n: X^i \subseteq (X^j \ominus nB)\}$
$M(X^i, X^j)$	$\cup_{n=0}^{N}(((X^i \cap X^j) \oplus nB) \cap ((X^i \cup X^j) \ominus nB))$
$M^{\Delta}(X^i, X^j)$	$\cap_{n=0}^{N}(((Xi \cap Xj) \oplus nB) \cup ((Xi \cup Xj) \ominus nB))$
$H(X/B)$	$-\sum_{n=0}^{N} P_n lnP_n$, where, $P_n = \frac{PS_n(X/B)}{A(X)}$, $PS_n(X/B) = A(XonB) \backslash A(Xo(n+1)B)$

Grayscale Skeletonization, Granulometries, Morphological Interpolations, Morphological Distances

Transformation	Equation
$SK(f)$	$\bigvee_{\forall n}(SK_n)$, where, $(SK_n) = \bigvee_{\forall n}(f \ominus nB) - (f \ominus nB) \circ B$
$H(f/B)$	$-\sum_{n=0}^{N} P_n ln P_n$, where, $P_n = \frac{PS_n(f/B)}{A(f)}$, $PS_n(f/B) = A(f \circ nB) - A(f \circ (n+1)B)$
$M(f^i, f^j)$	$\bigvee_{\forall n}\left((f^i \wedge f^j) \oplus nB) \wedge (f^i \vee f^j) \ominus nB)\right)$
$M^{\Delta}(f^i, f^j)$	$\bigwedge_{\forall n}\left((f^i \wedge f^j) \oplus nB) \vee (f^i \vee f^j) \ominus nB)\right)$
$d(f^i, f^j) = d(f^j, f^i)$	$min\{n: A(f^i \vee f^j) < A(f^i \wedge f^j) \oplus nB\}$
$e(f^i, f^j) = e(f^j, f^i)$	$min\{n: A(f^i \vee f^j) \ominus nB < A(f^i \wedge f^j)\}$

Mathematical Morphological Operations: Many Application Domains

Morphological Operator	Application domain	Major references
Binary and Grayscale Morphological Erosion, Dilation, Opening, Closing, Multiscale Morphological Operations	Petrology, GISci, Geosciences, Remote sensing	Serra (1982), Sagar (2013), Brunet and Sills (2017), Beucher (1990, 1999)
Geodesic Morphological Operations	Remote sensing, GISci, Geography, Petrology	Lantuejoul (1978), Lantuejoul and Beucher (1981), Sagar and Lim (2008), Challa et al (2017)
Hit-or-Miss Transformation	Geomorphology, Hydrology	Serra (1982), Tay et al (2005)
Morphological Thinning, Thickening, Pruning	Hydrology, Cartography	Soille (2003), Sagar (2013)
Morphological Skeletonization	Cartography, Hydrology, Geomorphology	Sagar et al (2000, 2003), Soille (2003)
Skeletonization by Zones of Influence and Weighted Skeletonization by Zones of Influence	Cartography, Hydrology, Geomorphology	Beucher (1990), Rajasekhara et al (2012), Sagar (2014)
Granulometries and Anti-Granulometries	Petrology, Geomorphology, Hydrology	Serra (1982), Sagar (2013), Tay et al (2005, 2007), Vardhan et al (2013)
Morphological Distances, Hausdorff Dilation (Erosion) Distances	GISci, Limnology, Biogeography, Spatial planning	Serra (1988), Sagar (2010, 2013), Sagar and Lim (2015a,b)
Morphological Interpolations and Extrapolations	Geophysics, Atmospheric science, Geology, Remote sensing, Cartography	Sagar (2010) Brunet and Sills (2017), Rajasekhara et al (2012), Sagar (2014), Sagar and Lim (2015a,b)
Watershed Transformation	Hydrology, Remote sensing, Mapping, Borehole studies, Seismic data processing	Beucher and Meyer (1992), Rivest et al (1992), Sagar (2007)

Overview

I. Digital Elevation Models (DEMs): An Important Source Data for Geoscientists

II. Mathematical Morphology: Notations, Equations, and Transformations

III. Mathematical Morphology in DEMs

- Skeletonization in DEMs and DEM Partitions
- Granulometries: Surficial roughness characterization/ quantification
- Geodesic Spectrum in Bottom Topography Studies
- Morphological Interpolations: Morphing of Source DEM into Target DEM
- Ranks for Pairs of Images; DEM Classification
- Morphological distances in spatial optimization and interaction modeling

IV. How the above studies could be integrated to better understand the surficial process dynamics?

III.I.I. Ridge-Valley Network Extraction from DEMs: Skeletonization

Functions (DEMs, Satellite Images, Microscopic Images etc)

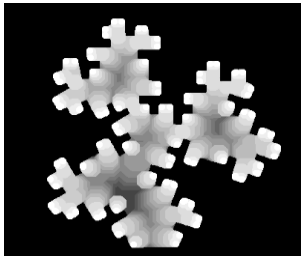

Sets (Thresholded Elevation regions, Binary images decomposed from images)

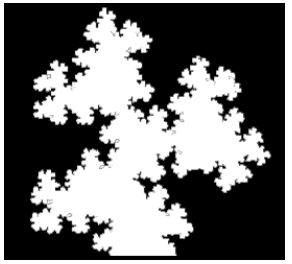

Skeletons (Unique topological networks)

B. S. Daya Sagar, M. Venu and D. Srinivas, 2000, Morphological operators to extract channel networks from Digital Elevation Models, International Journal of Remote Sensing. v. 21, no. 1, p. 21-30.

B. S. Daya Sagar, M. B. R. Murthy, C. Babu Rao and Baldev Raj, 2003, Morphological approach to extract ridge-valley connectivity networks from Digital Elevation Models (DEMs), International Journal of Remote Sensing, V. 24, No. 3, 573 – 581.

Network Extraction: Binary Morphology-Based

Threshold decomposition of f(x, y)

Step 2: **Skeletonization**

Systematic logical union and difference to extract network within each spatially distributed region and Union of network (s) obtained

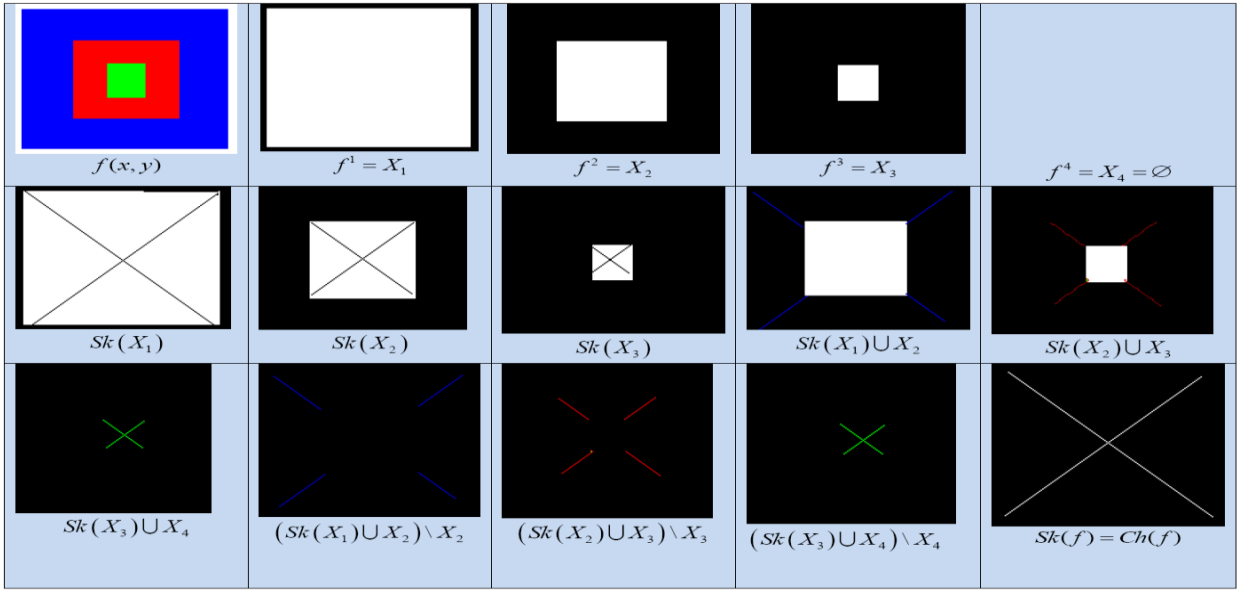

$$f^t = \begin{cases} 1 & if \quad f(x,y) \geq t \\ 0 & if \quad f(x,y) < t \end{cases} \quad where \quad 0 \leq f(x,y) \leq 255$$

$$f^t = X_t; f^{t+1} = X_{t+1}; \cdots; f^N = X$$

$$Sk_n(X_t) = (X_t \ominus nB) \setminus (X_t \ominus nB) \circ B \qquad n = 0,1,2,\cdots,N$$

$$Sk(X_t) = \bigcup_{n=0}^{N} Sk_n(X_t)$$

$$CH(f) = \bigcup_{t=1}^{255} \left(\left(Sk(X_t) \cup X_{t+1} \right) \setminus X_{t+1} \right)$$

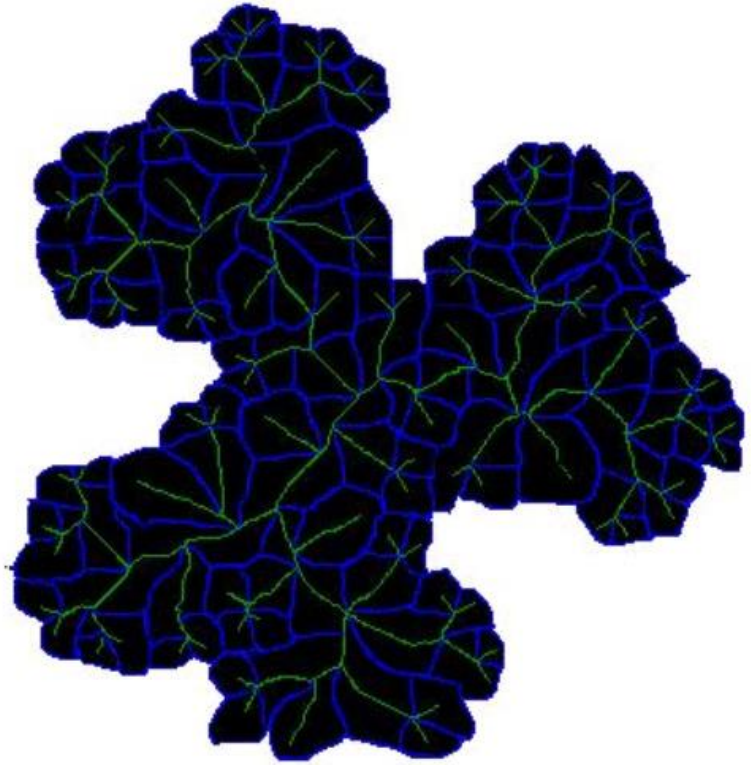

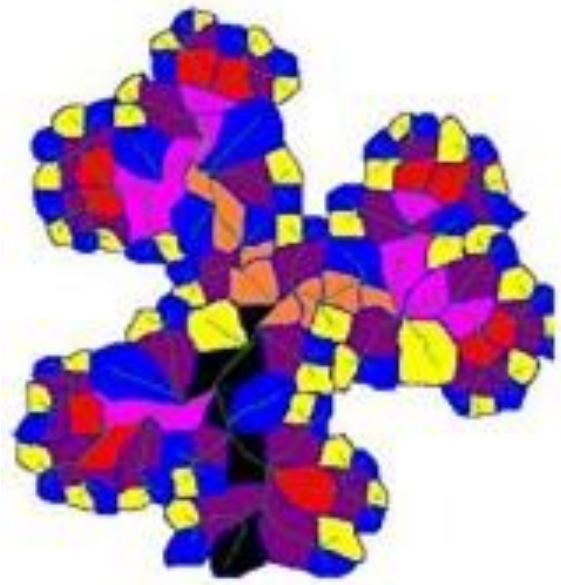

Binary morphology-based network extraction is: more stable, more accurate, and computationally expensive

Grayscale-based network extraction—may not be accurate like binary-morphology based—generates network that yields disconnections some times, but computationally not expensive.

Decomposed basins and networks

Networks : Binary Vs Grayscale

Binary Morphology

Binary morphology-based network extraction is:

- more stable,
- more accurate, and
- computationally expensive

Gray-scale Morphology

Grayscale-based network extraction—

- may not be accurate like binary-morphology based—
  - generates network that yields disconnections some times, but
- computationally not expensive.

III.I.II. Synthetic Fractal DEM and Unique Topological Networks: Reconstruction from Skeleton

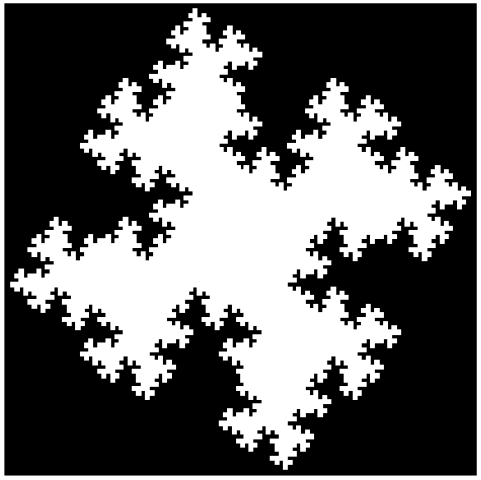

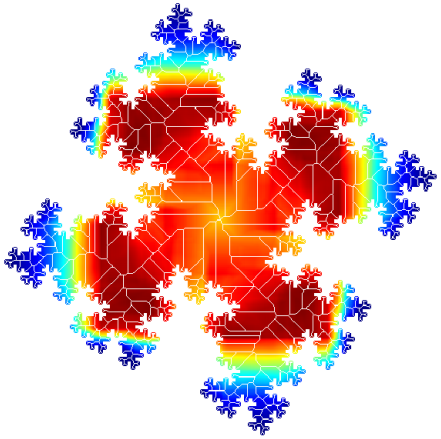

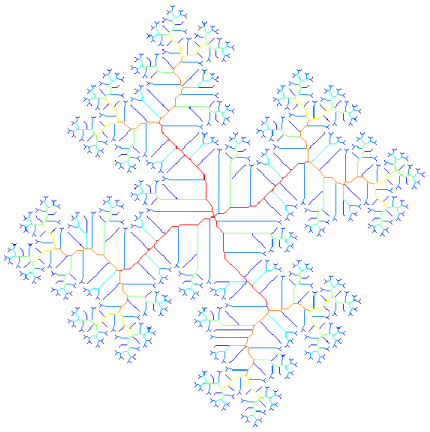

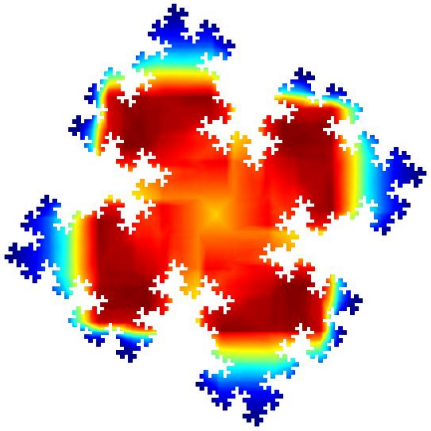

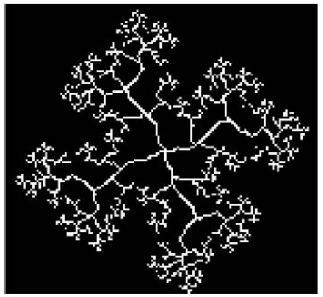

Fig. 2 Fluid FDN extracted from binary fractal basin.

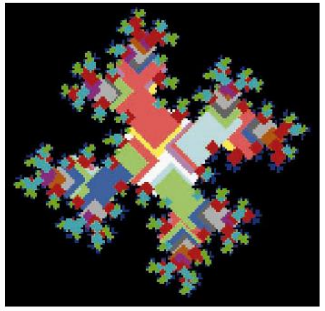

Fig. 3 A binary fractal basin after decomposition into TPRs.

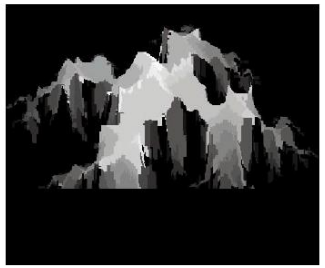

(a)

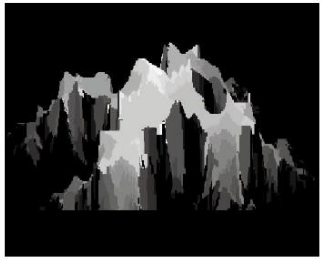

(b)

Fig. 4 A fractal landscape generated from Fig. 3. Light and dark regions of DEM are visualized as high and low elevations, respectively (vertical exaggeration: (a) 5 and (b) 7).

and (9), producing a transcendental DEM (Fig. 3) from binary fractal (Fig. 1). The binary fractal

B. S. Daya Sagar and K S R Murthy, 2000, Generation of fractal landscape using nonlinear mathematical morphological transformations, *Fractals*, v. 8, no. 3, p.267-272.

III.I.II. Synthetic Landscapes: Simulated DEM

Five main steps involved in the simulation are:

i. Successive erosion frontlines are generated *via* $(X \ominus Bn)$ by increasing the size of structuring element. Erosions are performed iteratively to generate erosion frontlines within a binary fractal basin.

ii. Smoothening of the erosion frontlines is achieved *via* $(X \ominus B\text{n}) \ominus \overset{\oplus}{B}]$ B. Here, the dilation combines the eroded version of the eroded binary basin achieved at step (i) and S.

iii. Various orders of network subset ranging from n=0 to N are isolated from each erosion frontline by subtracting the resultant information achieved in step (ii) from step (i).

iv. TPRs are generated by dilating the resultant information, which is achieved at step (iii) by Bn. This is an iterative procedure till the whole basin is converted into TPRs. Each TPR is assigned a specific value assuming that the spatially distributed TPRs are akin to spatially distributed elevation regions, and

v. Various orders of coded TPRs are combined to produce the simualted DEM. By employing these sequential steps, a self-affine fractal DEM is generated.

Overview

I. Digital Elevation Models (DEMs): An Important Source Data for Geoscientists

II. Mathematical Morphology: Notations, Equations, and Transformations

III. Mathematical Morphology in DEMs

- Skeletonization in DEMs and DEM Partitions
- Granulometries: Surficial roughness characterization/ quantification
- Geodesic Spectrum in Bottom Topography Studies
- Morphological Interpolations: Morphing of Source DEM into Target DEM
- Ranks for Pairs of Images; DEM Classification
- Morphological distances in spatial optimization and interaction modeling

IV. How the above studies could be integrated to better understand the surficial process dynamics?

III.II. Mathematical Morphology in Quantitative Analysis

I. **Scale invariant but shape-dependent (Morphological Shape Decomposition)**
II. **Roughness characterization (Granulometries)**

Scale Invariant but Shape-Dependent Measures

B. S. Daya Sagar and L. Chockalingam, 2004, Fractal dimension of non-network space of a catchment basin Geophysical Research Letters, v.31, no.12, L12502.

L. Chockalingam and B. S. Daya Sagar, 2005, Morphometry of networks and non-network spaces, Journal of Geophysical Research-Solid Earth, v. 110, B08203, doi:10.1029/2005JB003641.

Roughness Characterization

Lea Tien Tay, B. S. Daya Sagar and Hean Teik Chuah, 2007, Granulometric analysis of basin-wise DEMs: a comparative study, International Journal of Remote Sensing, 28, 15.

K. Nagajothi and B. S. Daya Sagar, Classification of Geophysical Basins Derived From SRTM and Cartosat DEMs via Directional Granulometries, IEEE Journal on Selected Topics on Applied Earth Observation and Remote Sensing, v. 12, no. 12, p. 5259-5267, 2019.

III.II.I. Scale Invariant but Shape-Dependent Measures (Morphological Shape Decomposition)

To propose morphology based method via fragmentation rules to compute scale invariant but shape-dependent measures of non-network space of a basin.

To make comparisons between morphometry based parameters / dimensions and dimensions derived for non-network space.

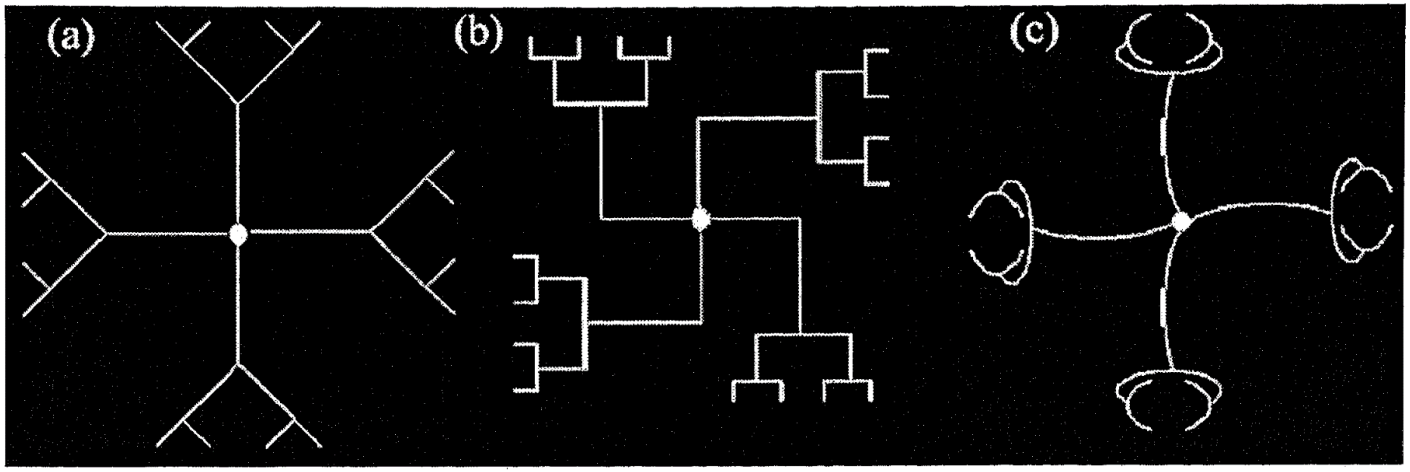

Topologically Invariant networks with variant geometric organization

Proposed Technique

Step1: Channel network is traced from topographic map.

Step2: Channel network is dilated and eroded iteratively until the entire basin is filled up with white space. This step is to generate catchment boundary automatically. Dilation followed by erosion is called structural closing, which will smoothen the image.

Step3: Generate the basin with channel network and non-network space with boundary by subtracting the channel network from the catchment boundary achieved in Step2.

Step4: Structural opening (erosion followed by dilation) is performed recursively in basin achieved in Step3 to fill the entire basin of non-network space with varying size of octagons.

Step5: Assign unique color for each size of octagons.

Step6: Compute morphometry for the basin.

Step7: Compute shape dependent dimensions.

Algorithm Implementation:

Step 1: **Channel network of sub basin 1**

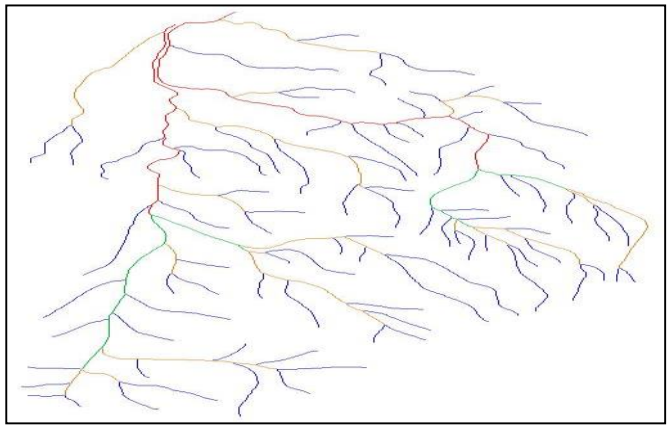

Step 2: **Close-Hull Generation**

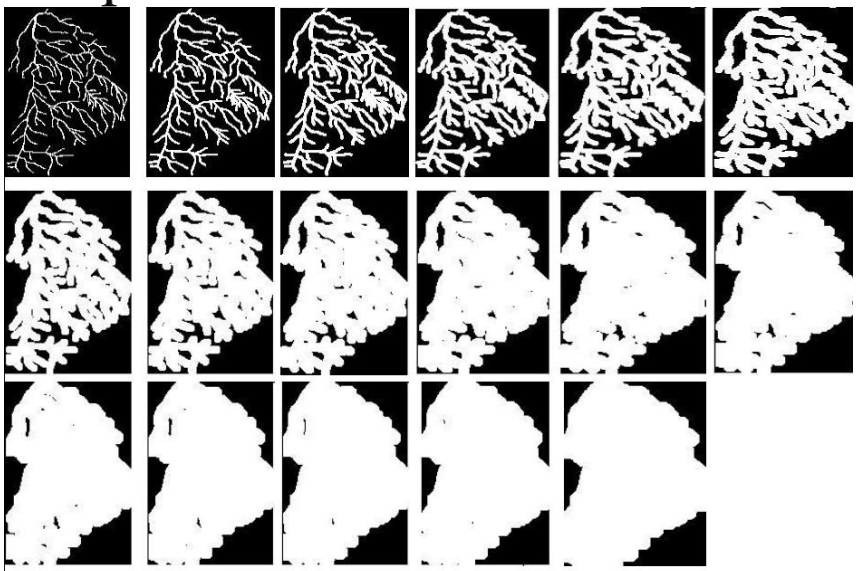

Iterative dilation of channel network of basin 1

Step 3: Non-network space of basin

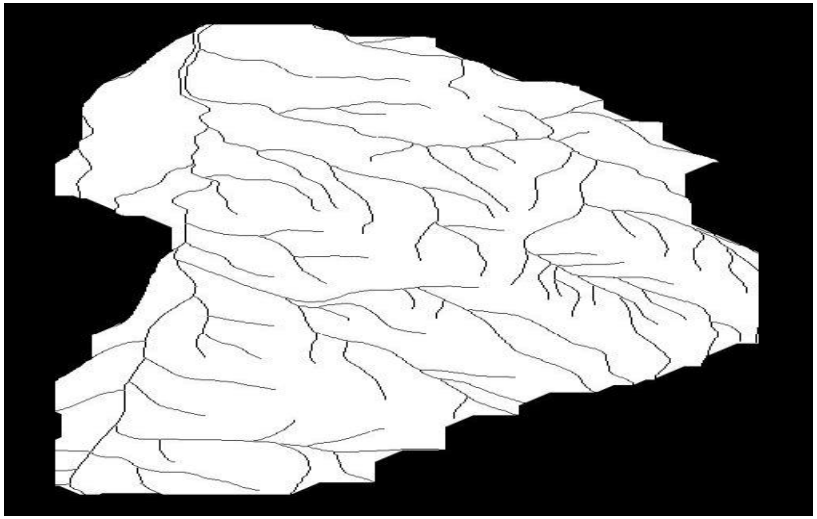

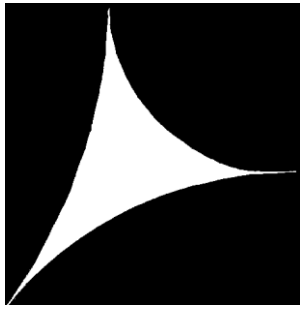

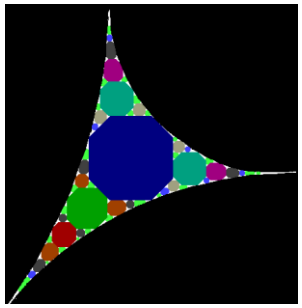

(a) Appollonian Space, and (b) after decomposition by means of octagon.

Non-Network Spaces Packed with Non-Overlapping Disks of basins 2 to 8

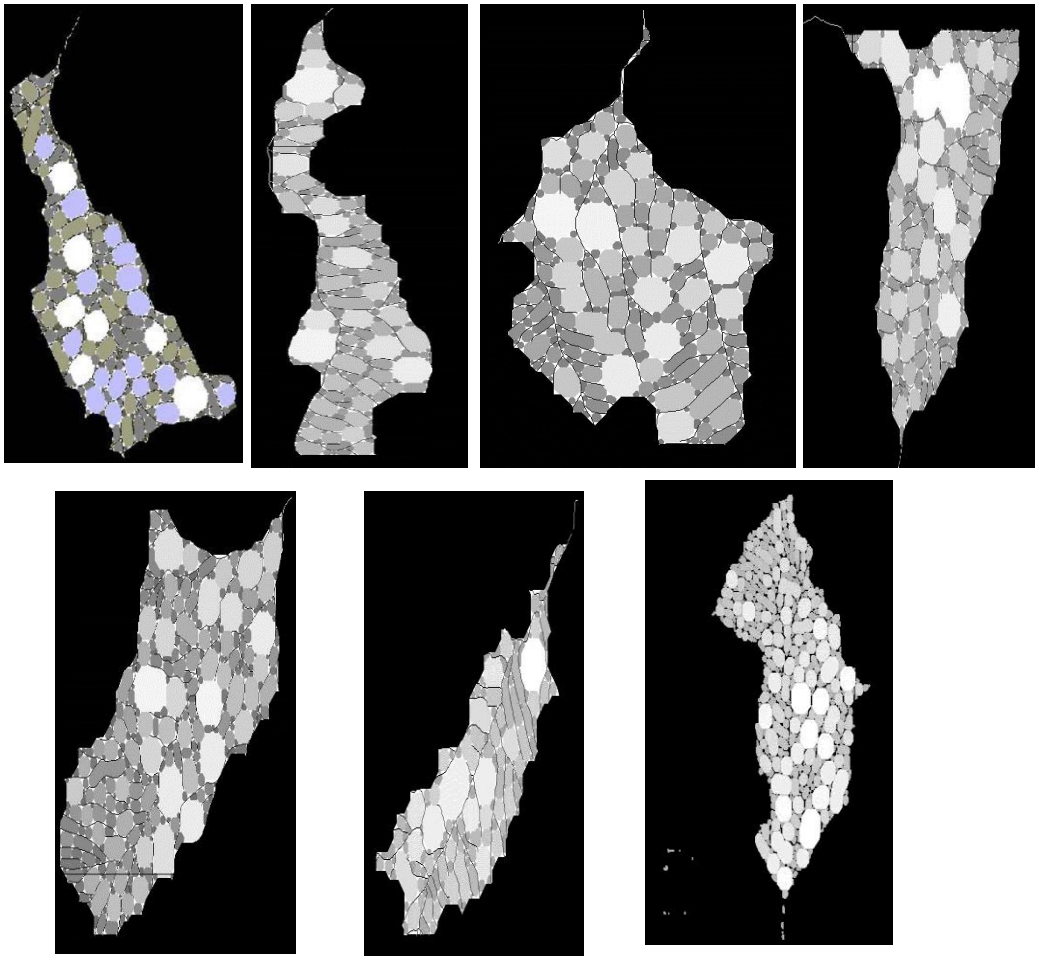

Decomposition of Non-network space in to non-overlapping disks of octagon shape of several sizes for basin 1

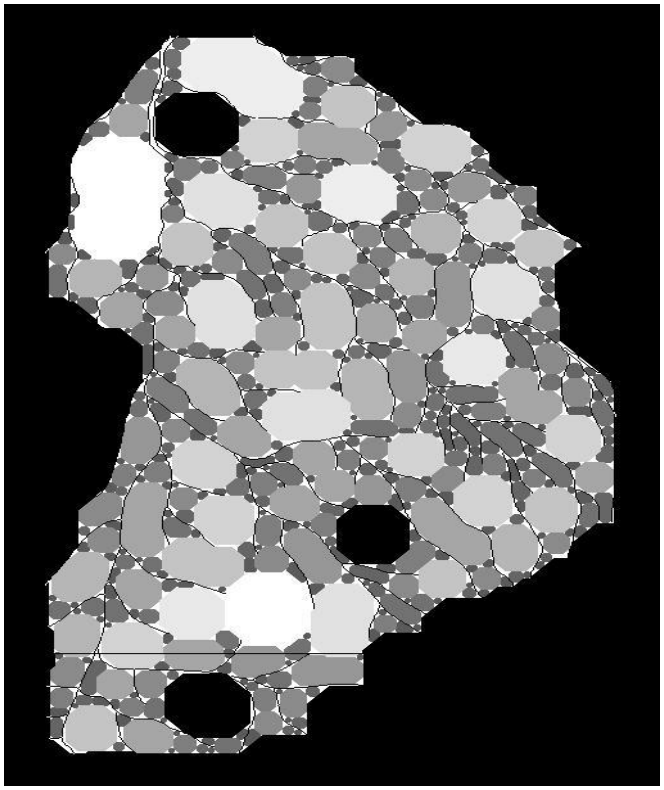

Dimensions derived from morphometry of network and non network space

Morphometric parameter computations achieved through decomposition of non-network space

Basin #	Network FD	Log R_S/ Log R_N	R vs A	R vs N	A vs N
1	1.83	1.93	1.34	2.06	1.50
2	0.86	1.63	1.33	1.23	1.59
3	0.98	1.41	1.02	1.87	1.80
4	2.07	2.01	1.43	2.17	1.52
5	1.73	1.90	1.34	1.94	1.43
6	1.84	2.04	1.13	1.87	1.63
7	1.33	1.61	1.23	2.08	1.70
8	1.65	2.06	1.61	2.38	1.49

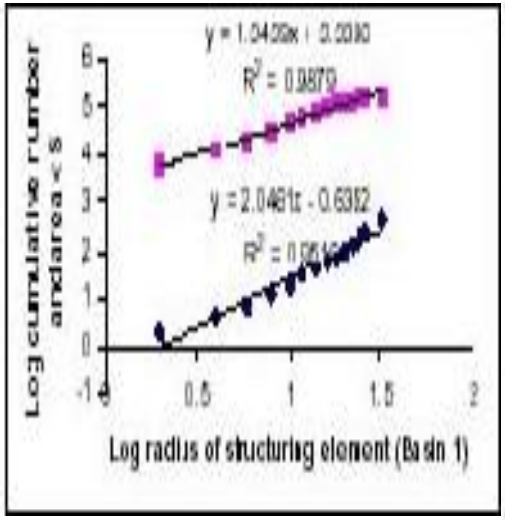

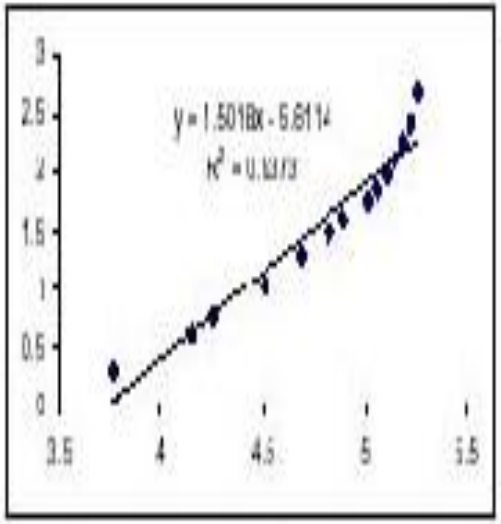

B. S. Daya Sagar and L. Chockalingam, 2004, Fractal dimension of non-network space of a catchment basin Geophysical Research Letters, v.31, no.12, L12502.

L. Chockalingam and B. S. Daya Sagar, 2005, Morphometry of networks and non-network spaces, Journal of Geophysical Research-Solid Earth, v. 110, B08203, doi:10.1029/2005JB003641.

III.II.II. **Roughness Characterization (Granulometries)**

Morphological multiscaling transformations are shown to be a potential tool in deriving meaningful terrain roughness indexes.

Consider two different basins of two different physiographic setups (fluvial and tidal) that possess similar topological quantities, i.e., their networks may be topologically similar to each other. But the processes involved therein may be highly contrasting due to their different physiographic origins. Under such circumstances, the results that exhibit similarities in terms of topological quantities and scaling exponents would be insufficient to make an appropriate relationship with involved processes.

Therefore, granulometric approach is proposed to derive shape-size complexity measures of basins. This approach is based on probability distribution functions computed for both protrusions and intrusions (in other words *supremums* and *infimums*) of various degrees of sub-basins.

This granulometry-based technique is tested on sub-basins with various sizes and shapes decomposed from DEMs of two distinct geomorphic regions.

Granulometric Analysis

- Multi-scale opening till completely black
- Multi-scale closing till completely white
- Subtraction
- Probability function

$$PS_f(-n, B) = A[(f \bullet B_n) - (f \bullet B_{n-1})], 1 \le n \le K$$

$$PS_f(+n, B) = A[(f \circ B_n) - (f \circ B_{n+1})], 0 \le n \le N$$

- Average size

$$ps(n, f) = \frac{A(f \circ B_n) - A(f \circ B_{n+1})}{A(f \circ B_0)}, n = 0,1,2,..., N$$

$$ps(-n, f) = \frac{A(f \bullet B_n) - A(f \bullet B_{n-1})}{A(f \bullet B_K) - A(f \bullet B_0)}, n = 1,2,..., K$$

$$AS(f / B) = \sum_{n=0}^{N} n ps(n, f)$$

- Average roughness

$$H(f / B) = -\sum_{k=0}^{n} ps(n, f) \log ps(n, f)$$

Anti(Granulometric) Analysis

Multiscale opening/closing by rhombus

- Scale 1 , 40, 80, 120, 160

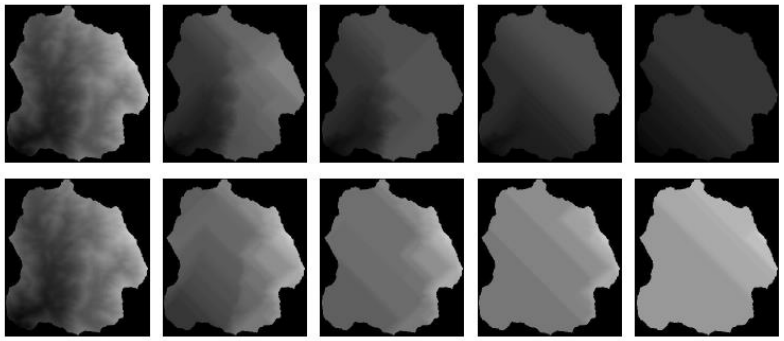

Multiscale opening/closing by square

- Scale 1 , 20, 40, 60, 80

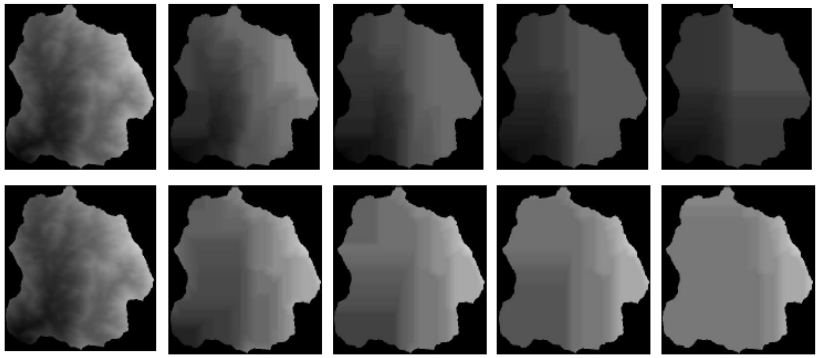

Multiscale opening/closing by octagon

- Scale 1 , 30, 60, 90, 120

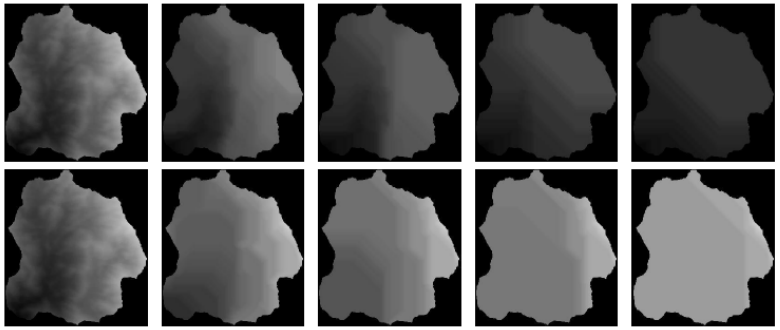

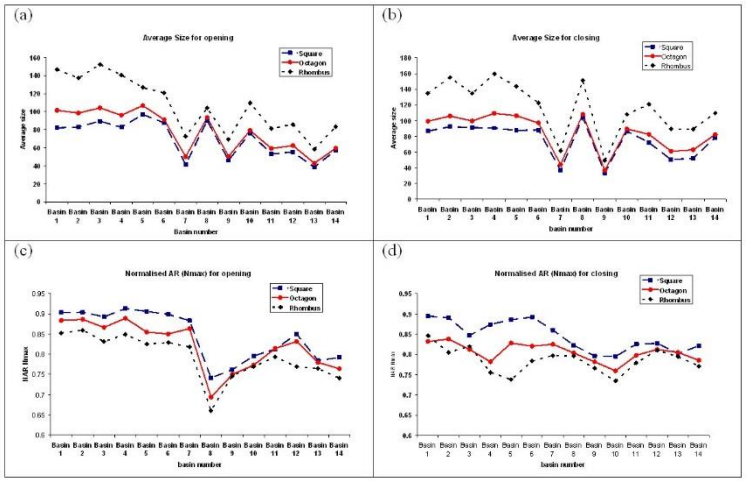

Average size and Average roughness – 14 sub-basins

Terrestrial Global and Directional Roughness: Cartosat DEM

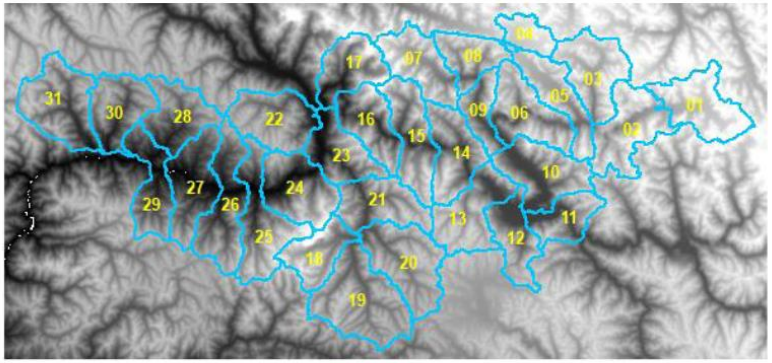

(c)

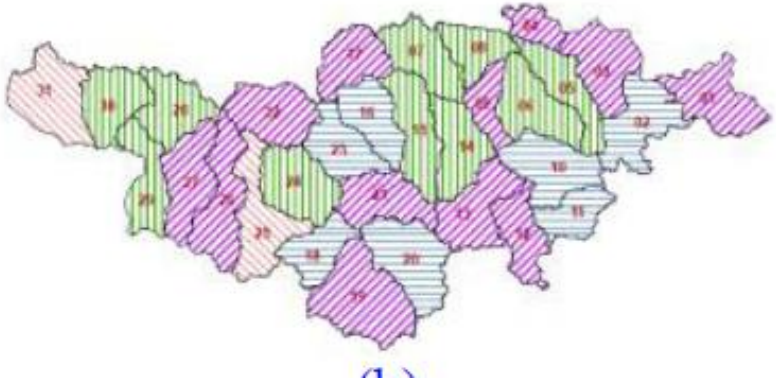

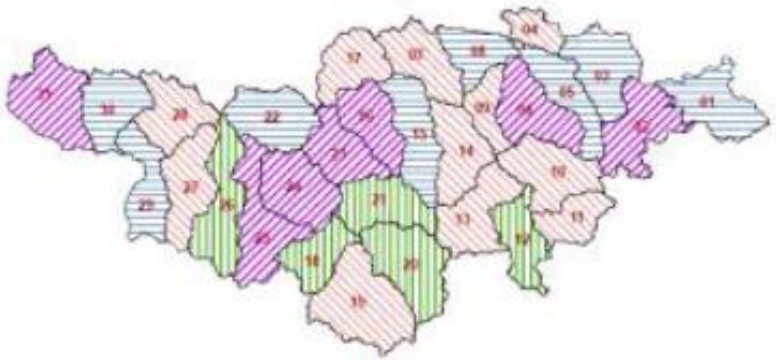

Terrestrial Surface

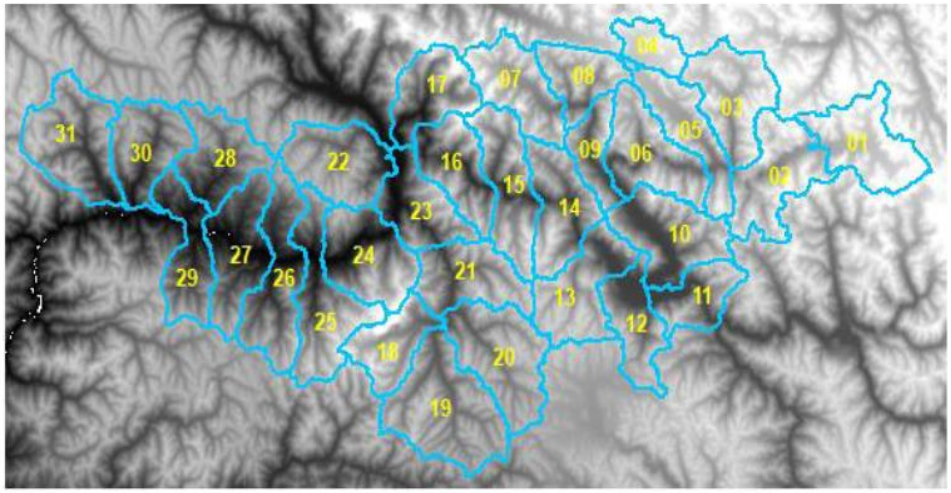

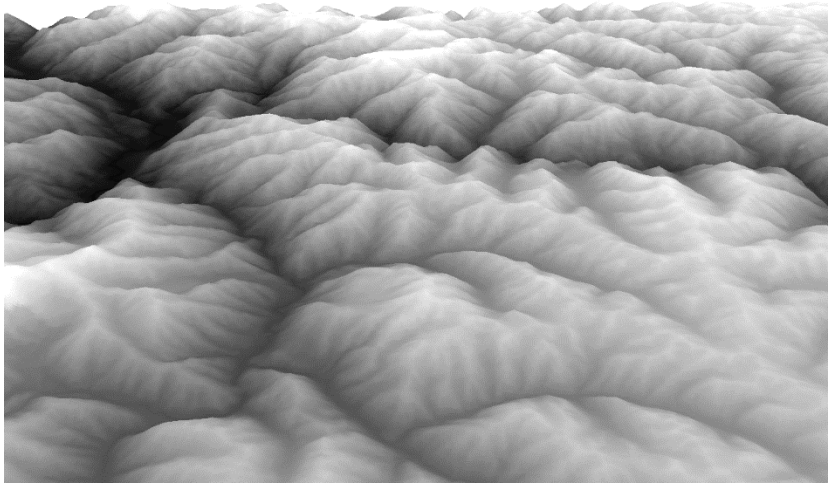

Lea Tien Tay, B. S. Daya Sagar and Hean Teik Chuah, 2007, Granulometric analysis of basin-wise DEMs: a comparative study, International Journal of Remote Sensing, 28, 15.

K. Nagajothi and B. S. Daya Sagar, Classification of Geophysical Basins Derived From SRTM and Cartosat DEMs via Directional Granulometries, IEEE Journal on Selected Topics on Applied Earth Observation and Remote Sensing, v. 12, no. 12, p. 5259-5267, 2019.

Lower-Indus basin shown in Fig. 1(a) after multiscale opening by (a) 10 cycles, (b) 100 cycles, (c) 1000 cycles, and (d) 10000 cycles.

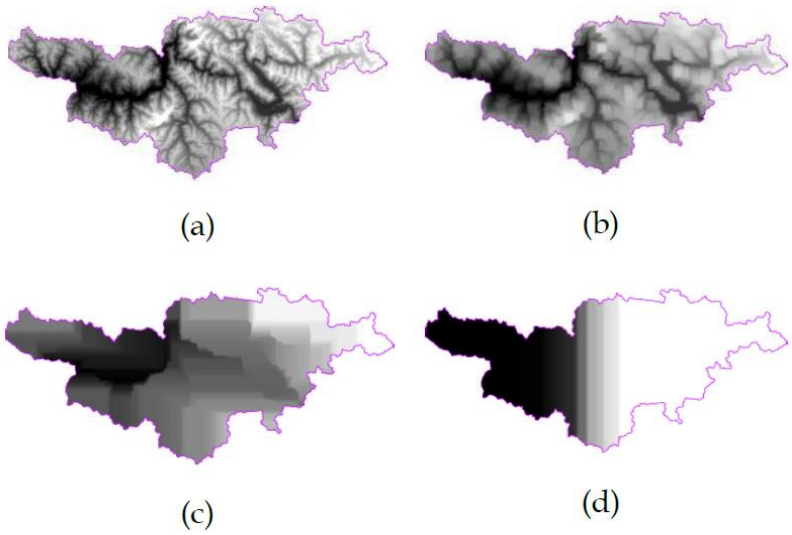

Lower-Indus subbasin subject to multiscale openings by (a) B^1, (b) B^2, (c) B^3, and (d) B^4 after 100 cycles of morphological opening.

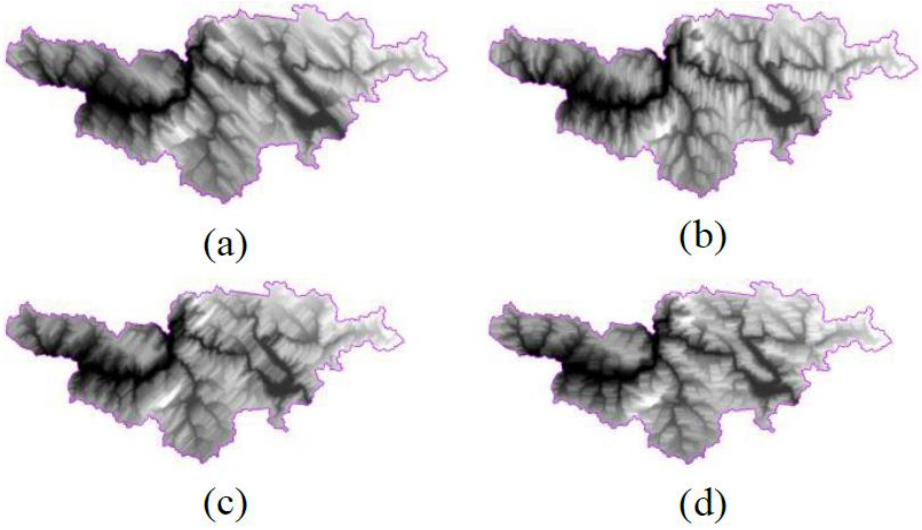

Evolution of watershed-19 under recursive opening cycles with respect to B, B^1, B^2, B^3 and B^4

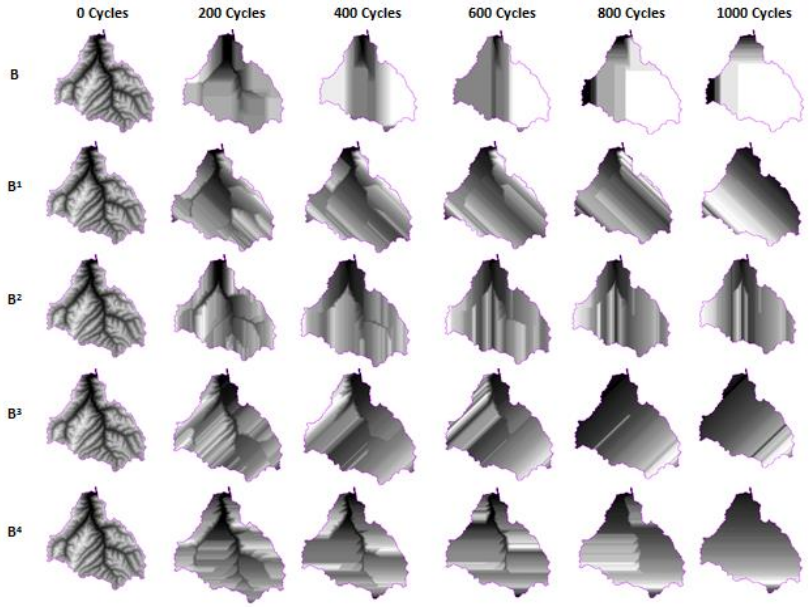

Behaviors of watersheds from Carto-1 DEM under multiscale opening of (a) f^{31} by B^1, (b) f^7 by B^2, (c) f^4 by B^3, and (d) f^{18} by B^4, at the cycles 0,50,100,150 & 200.

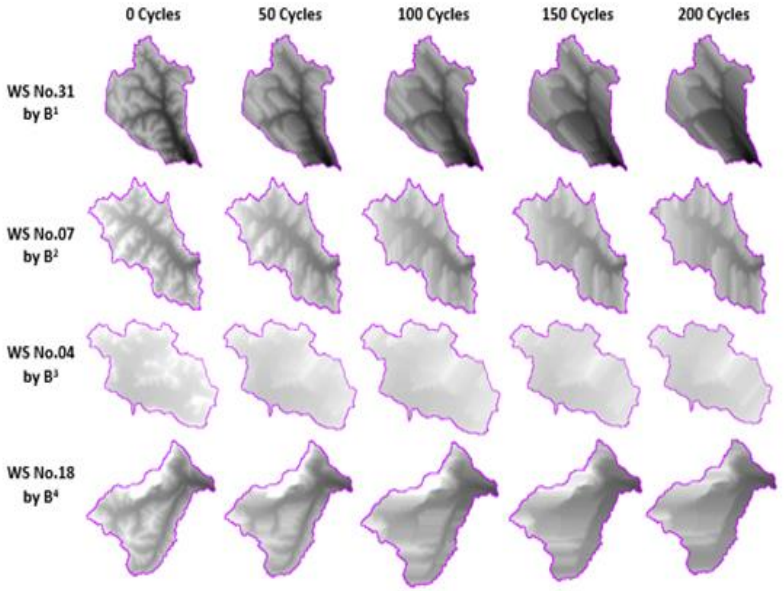

Normalized Granulometric Indices Carto-1 DEM. Categories : (1) 0-0.25, (2) 0.26-5.0, (3) 0.51-0.75, (4) 0.76-1.0.

Low directional granulometric index values of 31 watersheds derived from Cartosat-1 DEM

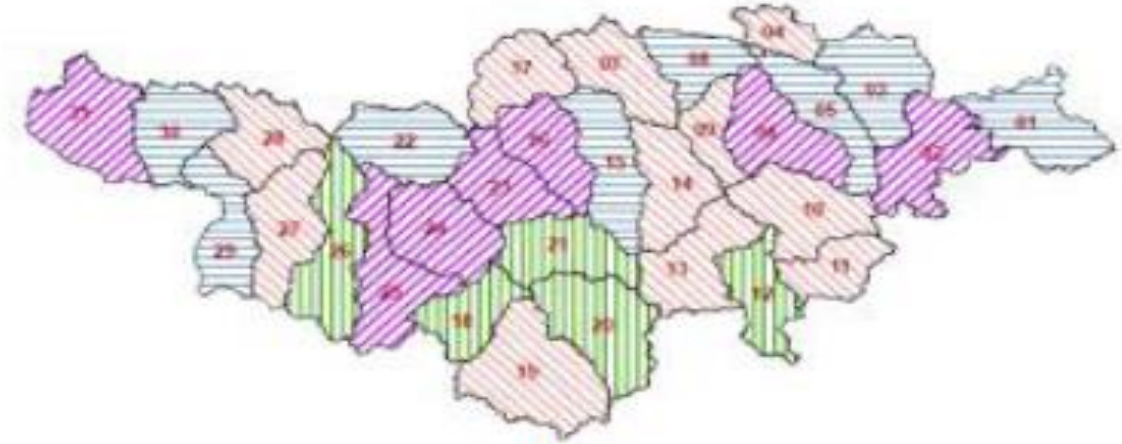

Granulometric Analysis : Basin wise analysis

The number of iterations required to make each sub-basin either become darker or brighter depends on the size, shape, origin, orientation of considered primitive template used to perform multiscale openings or closings, and also on the size of the basin and its physiographic composition. More opening/closing cycles are needed when structuring element rhombus is used, and it is followed by octagon and square.

Mean roughness indicates the shape-content of the basins. If the shape of SE is geometrically similar to basin regions, the average roughness result possesses lower analytical values. If the topography of basin is very different from the shape of SE, high roughness value is produced, which indicates that the basin is rough relative to that SE. In general, all basins are rougher relative to square shape as highest roughness indices are derived when square is used as SE.

A clear distinction is obvious between the Cameron and Petaling basins. Generally, roughness values of Cameron basins are significantly higher than that of Petaling basins.

The terrain complexity measures derived granulometrically are scale-independent, but strictly shape-dependent. The shape dependent complexity measures are sensitive to record the variations in basin shape, topology, and geometric organisation of hillslopes.

Granulometric analysis of basin-wise DEMs is a helpful tool for defining roughness parameters and other morphological/topological quantities.

Overview

I. Digital Elevation Models (DEMs): An Important Source Data for Geoscientists

II. Mathematical Morphology: Notations, Equations, and Transformations

III. Mathematical Morphology in DEMs

- Skeletonization in DEMs and DEM Partitions
- Granulometries: Surficial roughness characterization/ quantification
- Geodesic Spectrum in Bottom Topography Studies
- Morphological Interpolations: Morphing of Source DEM into Target DEM
- Ranks for Pairs of Images; DEM Classification
- Morphological distances in spatial optimization and interaction modeling

IV. How the above studies could be integrated to better understand the surficial process dynamics?

III.III. Geodesic Spectrum in Bottom Topography Studies

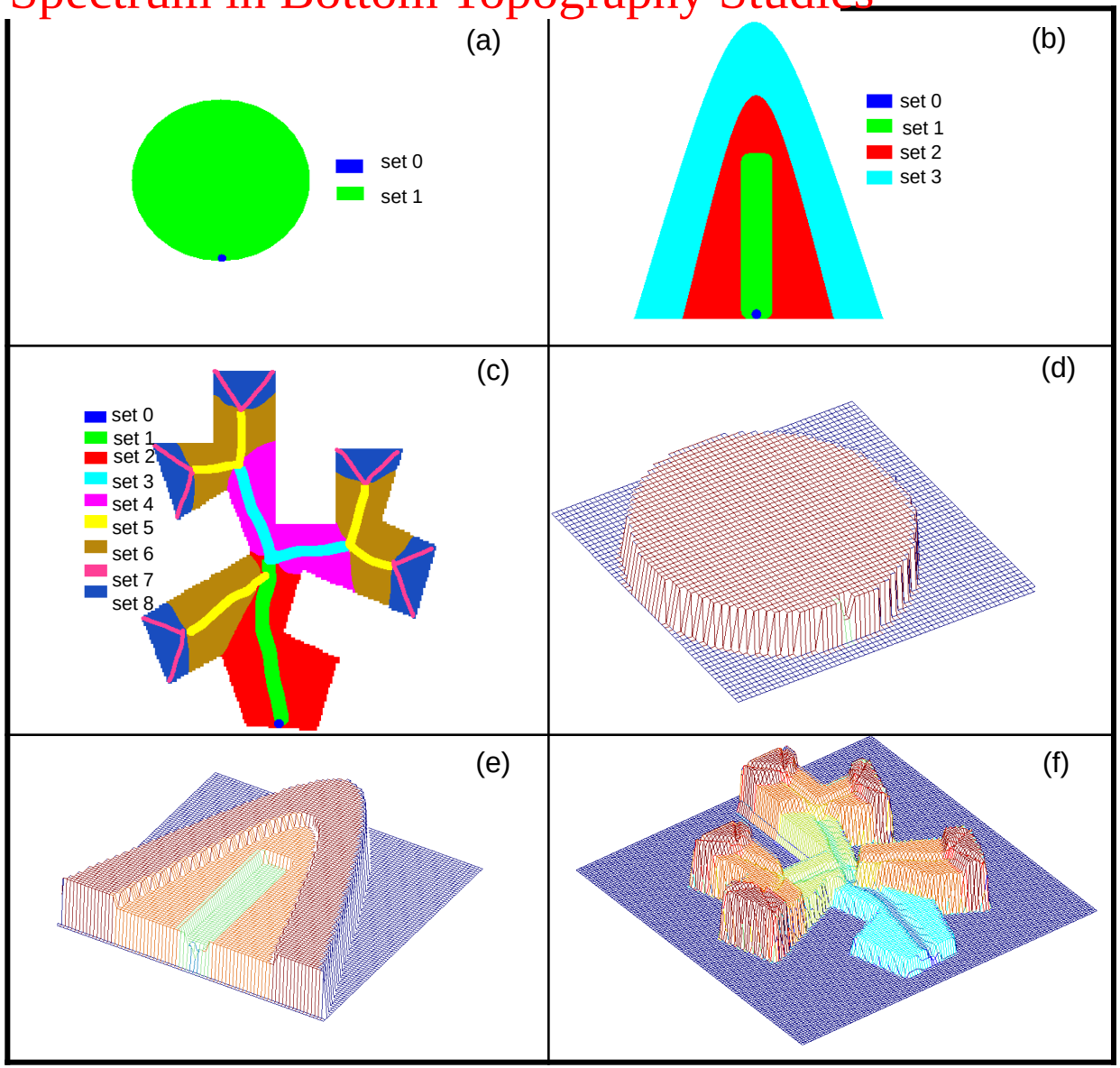

Fig 1.5 Tidal basins with different assumptions: (a) flat tidal basin, (b) tidal basin with a channelized and nonchannelized zones (multiple sets of topological significance), and (c) tidal basin with multiple sets, sets indexed with even and odd indexes, respectively, refer to channelized and nonchannelized zones. (d)–(f) 3D mesh representation of three synthetic tidal basin shown in (a)-(c).

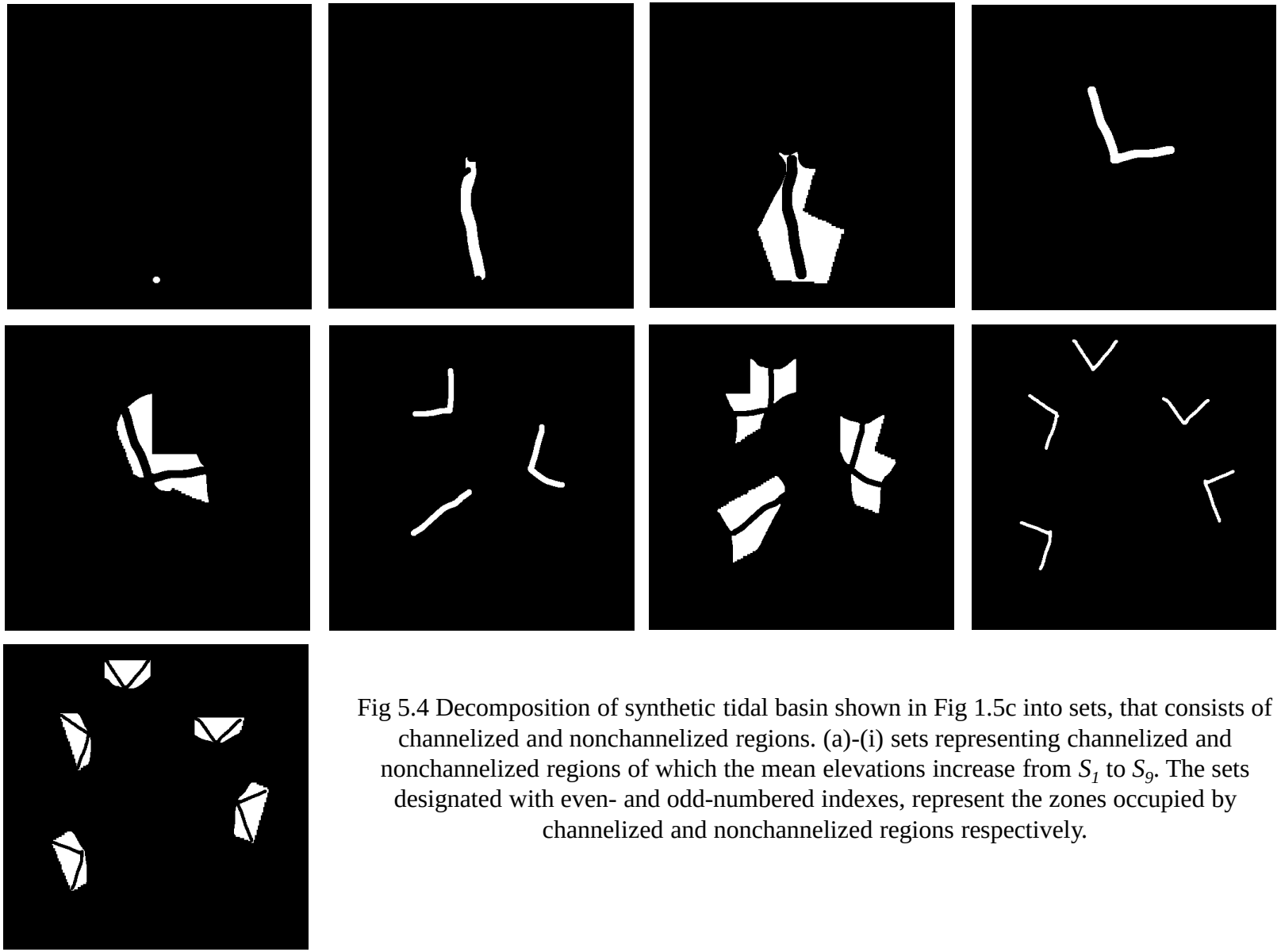

Fig 5.4 Decomposition of synthetic tidal basin shown in Fig 1.5c into sets, that consists of channelized and nonchannelized regions. (a)-(i) sets representing channelized and nonchannelized regions of which the mean elevations increase from S_1 to S_9. The sets designated with even- and odd-numbered indexes, represent the zones occupied by channelized and nonchannelized regions respectively.

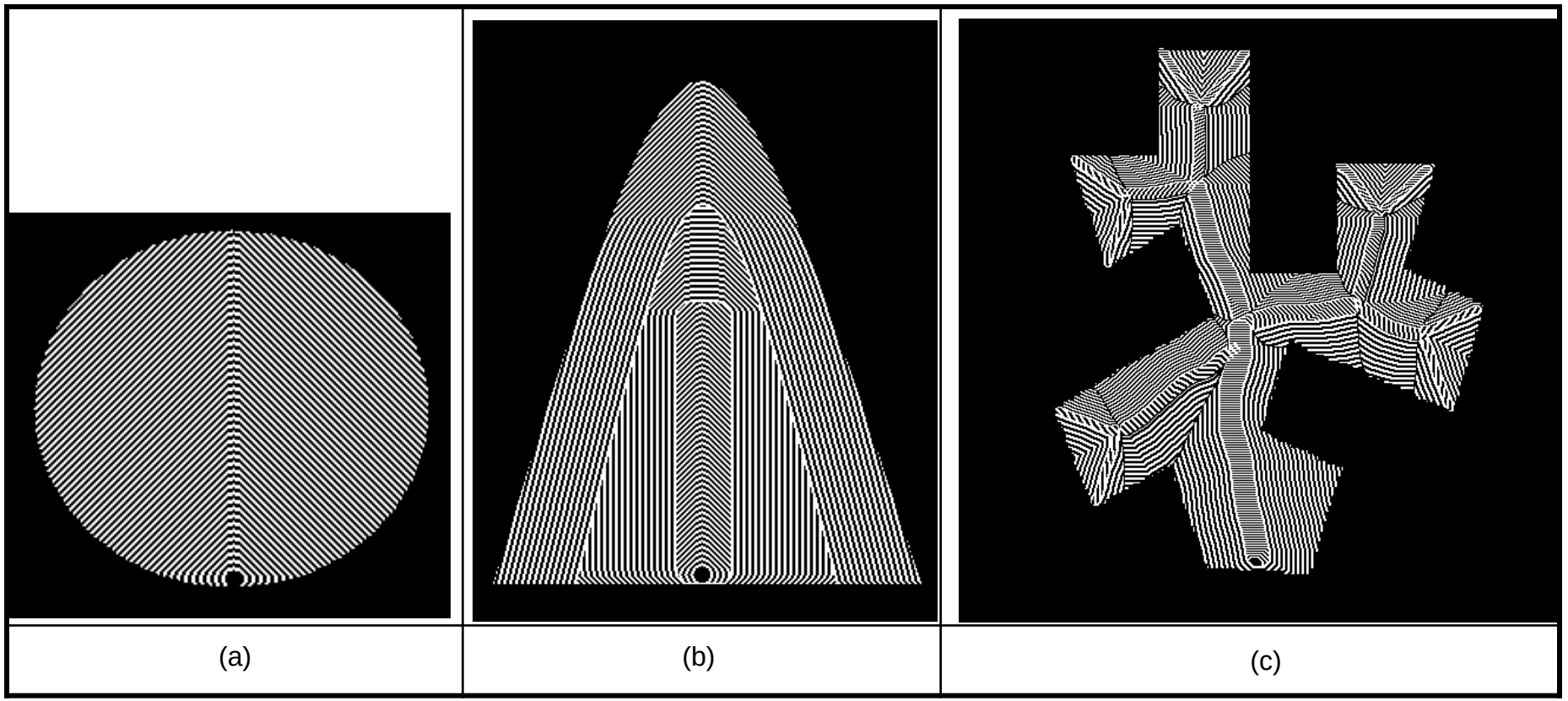

Fig 5.5 (a) Flow fields with isotropic propagation, (b) isotropic flow fields, and orthogonality between the flow fields of channelized and nonchannelized zones is obvious, and (c) flow fields within the tidal basin.

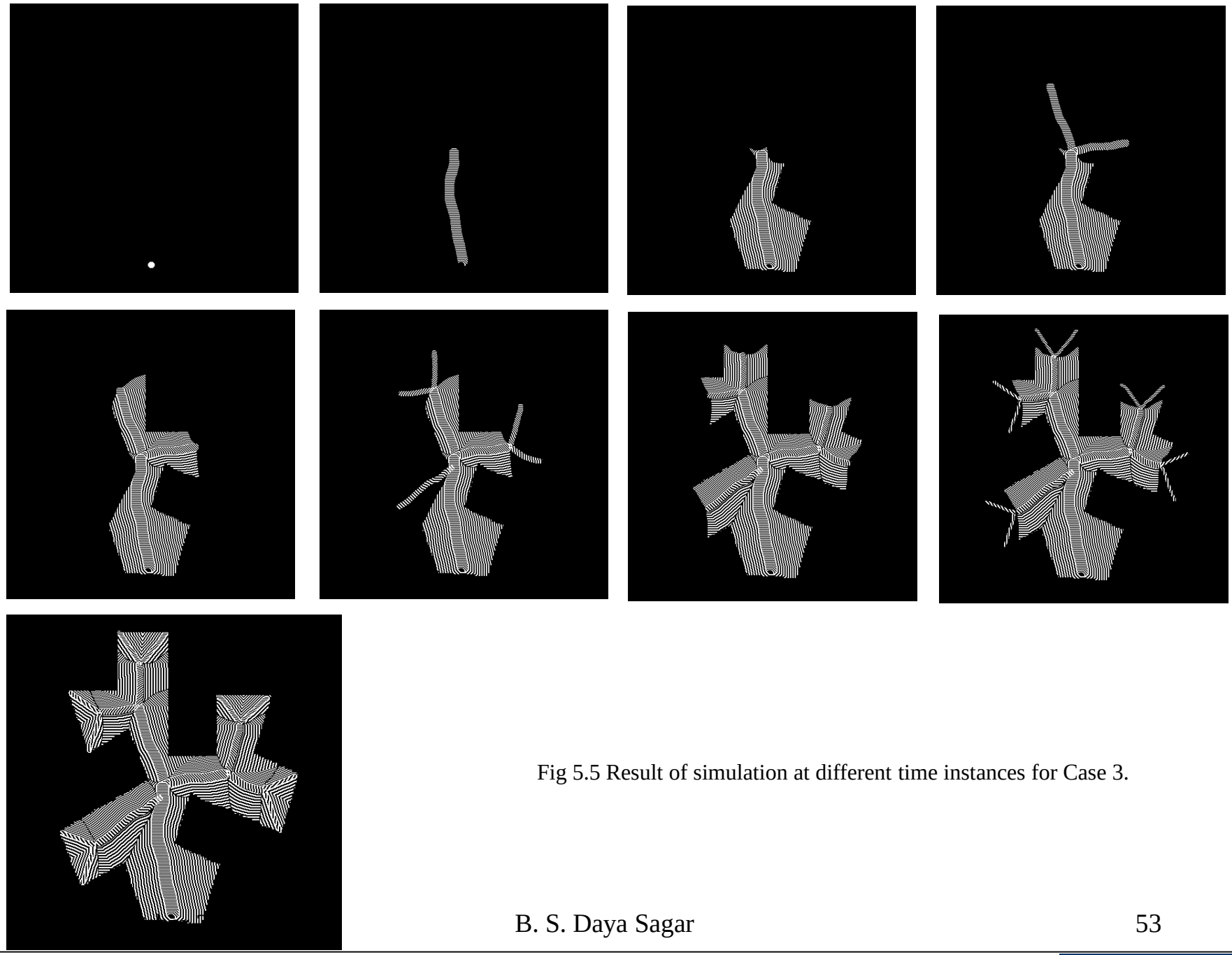

Fig 5.5 Result of simulation at different time instances for Case 3.

(a)

(b)

(c)

Fig (a) 3D view of remote sensing data of Central San Francisco Bay, (b) bathymetry of Central San Francisco Bay, (c) bathymetry of inset of (b).

(a)

(b)

Fig (a) 3D view of Santa Cruz, and (b) Digital elevation map of Santa Cruz.

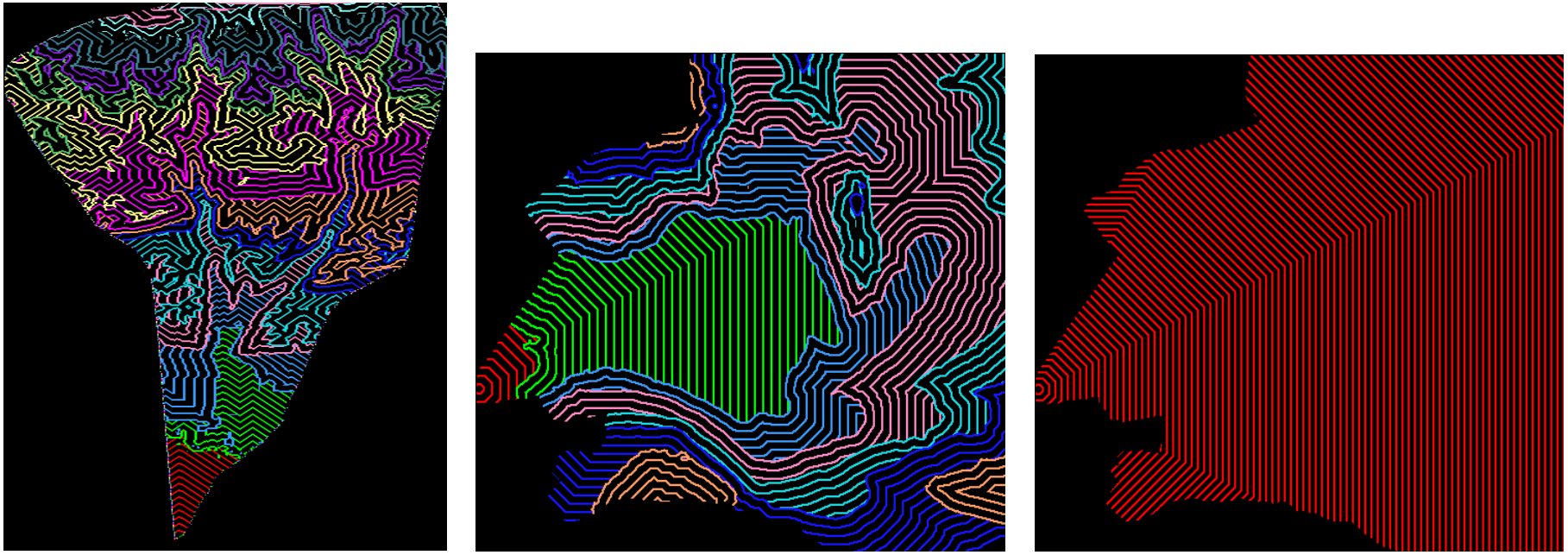

(a) (b) (c)

Fig (a) Flow field simulated on Santa Cruz DEM by using octagon structuring element, (b) flow field simulated on San Francisco Bay bathymetry by using octagon structuring element, and (c) flow field simulated on San Francisco Bay without considering bathymetry.

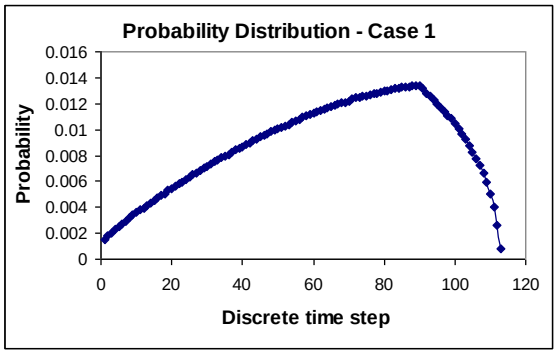

(a)

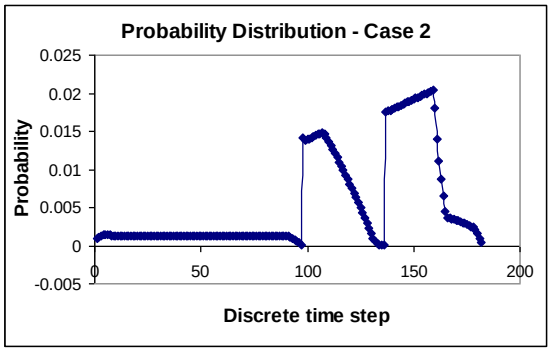

(b)

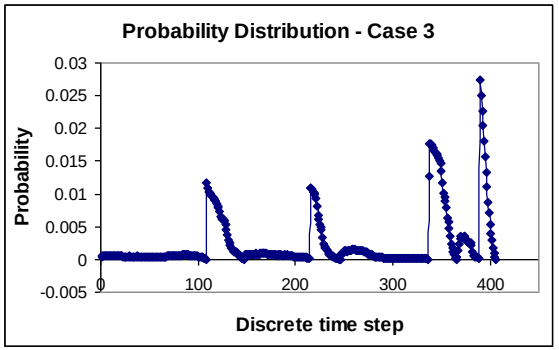

(c)

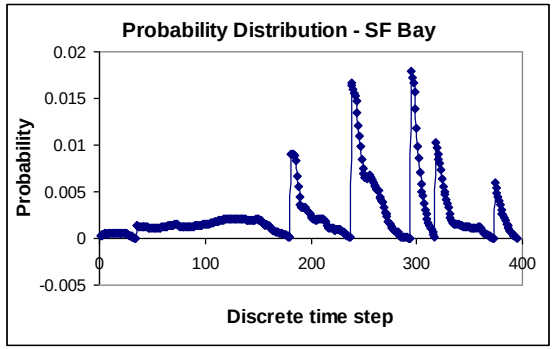

(d)

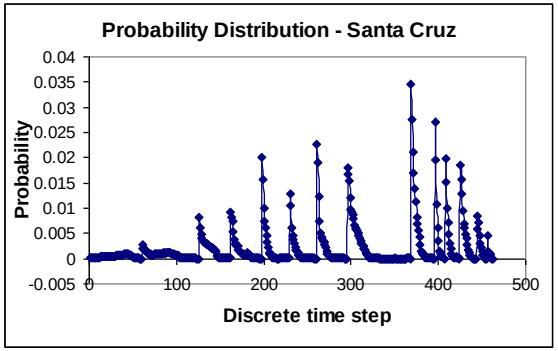

(e)

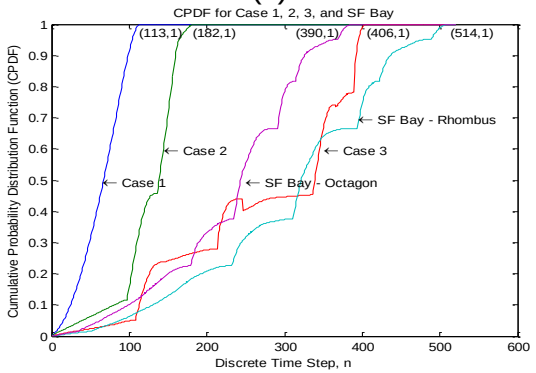

(f)

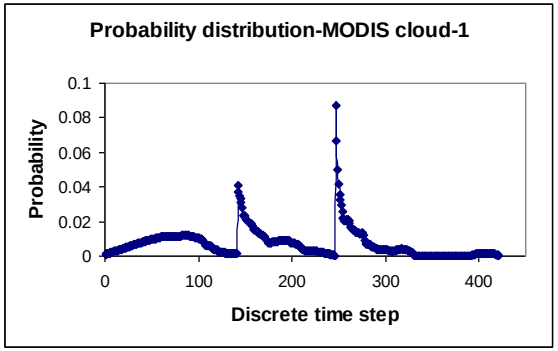

(g)

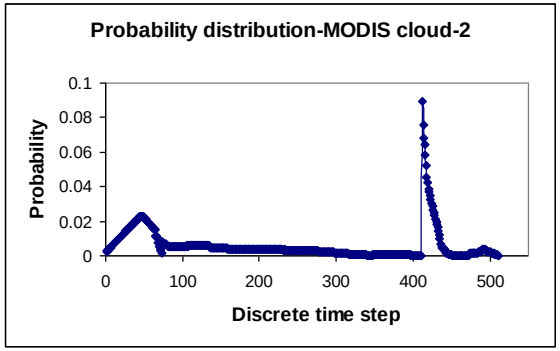

(h)

Figure Probability of estimated area flooded/propagated at each discrete time step.

Overview

I. Digital Elevation Models (DEMs): An Important Source Data for Geoscientists

II. Mathematical Morphology: Notations, Equations, and Transformations

III. Mathematical Morphology in DEMs

Skeletonization in DEMs and DEM Partitions

Granulometries: Surficial roughness characterization/ quantification

Geodesic Spectrum in Bottom Topography Studies

Morphological Interpolations: Morphing of Source DEM into Target DEM

Ranks for Pairs of Images; DEM Classification

Morphological distances in spatial optimization and interaction modeling

IV. How the above studies could be integrated to better understand the surficial process dynamics?

III.IV. Mathematical Morphological Interpolations: Different Scenarios

B. S. Daya Sagar, 2010, Visualization of spatiotemporal behavior of discrete maps via generation of recursive median elements, *IEEE Transactions on Pattern Analysis and Machine Intelligence*, vol. 32, no. 2, p. 378-384.

B. S. Daya Sagar, and Lim, S. L.: Morphing of grayscale DEMs via morphological interpolations, *IEEE Journal on Selected Topics on Applied Earth Observation and Remote Sensing*, 8, 11, 5190-5198, 2015.

B. S. Daya Sagar, and Lim, S. L.: Ranks for pairs of spatial fields via metric based on grayscale morphological distances, *IEEE Transactions on Image Processing*, 24, **3**, 908-918, 2015.

Aditya Challa, Sravan Danda, B. S. Daya Sagar, and Laurent Najman, Some Properties of Interpolations Using Mathematical Morphology, IEEE Transactions on Image Processing, 27, 4, 2038-2048, 2018.

Watersheds, SKIZ & WSKIZ

B. S. Daya Sagar, Universal scaling laws in surface water bodies and their zones of influence, *Water Resources Research*, v. 43, no. 2, W02416, 2007.

K. Nagajothi, H. M. Rajashekara, and B. S. Daya Sagar, 2021, Universal Fractal Scaling Laws for Surface Water Bodies and Their Zones of Influence, *IEEE Geoscience and Remote Sensing Letters*, (In Press), 10.1109/LGRS.2020.2988119

Rajashekara, H. M., Vardhan, P., and **B. S. Daya Sagar**, Generation of zonal map from point data via weighted skeletonization by influence zone, *IEEE Geoscience and Remote Sensing Letters*, 9, **3**, 403-407, 2012.

B. S. Daya Sagar, Cartograms via mathematical morphology, *Information Visualization*, 13, **1**, 42-48, 2014.

Grayscale Morphological Interpolations

$$\left(f^i \wedge f^j\right) = \inf\left(f^i, f^j\right) = \min\left\{f^i(x,y), f^j(x,y)\right\}$$

$$\left(f^i \vee f^j\right) = \sup\left(f^i, f^j\right) = \max\left\{f^i(x,y), f^j(x,y)\right\}$$

$$M\left(f^i, f^j\right) = \bigvee_{n=0}^{N}\left(M_n\left(f^i, f^j\right)\right)$$

where

$$M_n\left(f^i, f^j\right) = \left(\left(f^i \wedge f^j\right) \oplus nB\right) \wedge \left(\left(f^i \vee f^j\right) \ominus nB\right)$$

$$M_n\left(f^i, f^j\right) = \left(\left(f^i \wedge f^j\right) \oplus ng\right) \wedge \left(\left(f^i \vee f^j\right) \ominus ng\right)$$

3.2. Algorithm for Morphological median

Step 1. Consider f^i and f^j as the two spatial fields between which the morphological median needed to be computed.

Step 2. Register f^i and f^j by choosing appropriate control points such that f^i and f^j are with similar image size specifications.

Step 3. Compute the $\left(f^i \wedge f^j\right)$ and $\left(f^i \vee f^j\right)$

Step 4. Dilate the $\left(f^i \wedge f^j\right)$ for n-cycles, $\left(f^i \wedge f^j\right) \oplus nB$.

Step 5. Erode the $\left(f^i \vee f^j\right)$ for n-cycles, $\left(\left(f^i \vee f^j\right) \ominus nB\right)$,

Step 6. Compute the infima between the $\left(\left(f^i \wedge f^j\right) \oplus nB\right)$ and $\left(\left(f^i \vee f^j\right) \ominus nB\right)$, and denote it as $M_n\left(f^i, f^j\right)$.

Step 7. compute the area of $M_n\left(f^i, f^j\right)$, and denote it as $A\left(M_n\left(f^i, f^j\right)\right)$

Step 8. Repeat steps 4 through 7 for different n values until the $A\left(M_n\left(f^i, f^j\right)\right)$ becomes equivalent to $A\left(M_{n+1}\left(f^i, f^j\right)\right)$

Step 9. Take the suprema of $M_n\left(f^i, f^j\right)$ for all n-values, and denote it as $M\left(f^i, f^j\right)$.

By replacing flat structuring element (B) with non-flat structuring element (g) in the above nine steps, one can generate morphological median with respect to g.

Morphological Interpolations via Numerical Illustrations

(a)

194	168	9
190	44	71
101	181	12

(b)

25	81	112
210	243	98
178	9	196

Fig. 1. (a-b) Spatial fields.

(a)

25	81	9
190	44	71
101	9	12

(b)

194	168	112
210	243	98
178	181	196

Fig. 4. (a) infima and (b) suprema of two spatial fields shown in figure 1a and 1b.

(a)

190	81	81
190	190	71
190	101	71

(b)

168	112	98
178	98	98
178	178	98

(c)

168	81	81
178	98	71
178	101	71

(d)

191	191	190
191	191	191
191	191	190

(e)

98	98	97
97	97	97
98	97	97

(f)

98	98	97
97	97	97
98	97	97

(g)

190	190	190
190	190	190
190	190	190

(h)

98	98	98
98	98	98
98	98	98

(i)

98	98	98
98	98	98
98	98	98

(j)

168	98	98
178	98	98
178	101	98

Fig. 5. Generation of morphological medians generated by flat structuring element, between the two spatial fields shown in figure 1a and 1b. (a) dilation of infima shown in figure 4a, (b) erosion of suprema shown in figure 4b by 3x3 flat B, (c) infima between figure 5a and 5b, (d) dilation of infima shown in figure 4a by 5x5 flat B, (e) erosion of suprema shown in figure 4b by 5x5 flat B, (f) infima between figure 5d and 5e, (g) dilation of infima shown in figure 4a by 7x7 flat B, (h) erosion of suprema shown in figure 4b by 7x7 flat B, (i) infima between figure 5g and 5h, and (j) suprema of figures 5c, 5f, and 5i is considered as a morphological median between the two spatial fields (Fig. 1a and 1b), M(f^*, f^*).

(a)

191	190	82
192	191	81
191	190	72

(b)

167	98	97
168	97	96
176	98	97

(c)

167	98	82
168	97	81
176	98	72

(d)

192	191	190
193	192	191
192	191	190

(e)

98	97	96
97	96	95
98	97	96

(f)

98	97	96
97	96	95
98	97	96

(g)

193	192	191
194	193	192
193	192	191

(h)

97	96	95
96	95	94
97	96	95

(i)

97	96	95
96	95	94
97	96	95

(j)

167	98	96
168	97	95
176	98	96

Fig. 6. Generation of morphological medians generated by non-flat structuring element, between the two spatial fields shown in figure 1a and 1b. (a) dilation of infima shown in figure 4a, (b) erosion of suprema shown in figure 4b by 3x3 non-flat (g), (c) infima between figure 6a and 6b, (d) dilation of infima shown in figure 4a by 5x5 non-flat (g), (e) erosion of suprema shown in figure 4b by 5x5 non-flat (g), (f) infima between figure 6d and 6e, (g) dilation of infima shown in figure 4a by 7x7 non-flat (g), (h) erosion of suprema shown in figure 4b by 7x7 non-flat (g), (i) infima between figure 6g and 6h, and (j) suprema of figures 6c, 6f, and 6i is considered as a morphological median between the two spatial fields (Fig. 1a and 1b), M(f^*, f^*).

Morphological Interpolation: Earth Surface Transformation

Hierarchical Morphological Interpolation between landscape functions, say, f_1 and f_{256}.

f_1 f_{256}

f_{128}

f_{64} f_{192}

f_{32} f_{96} f_{160} f_{224}

⋮

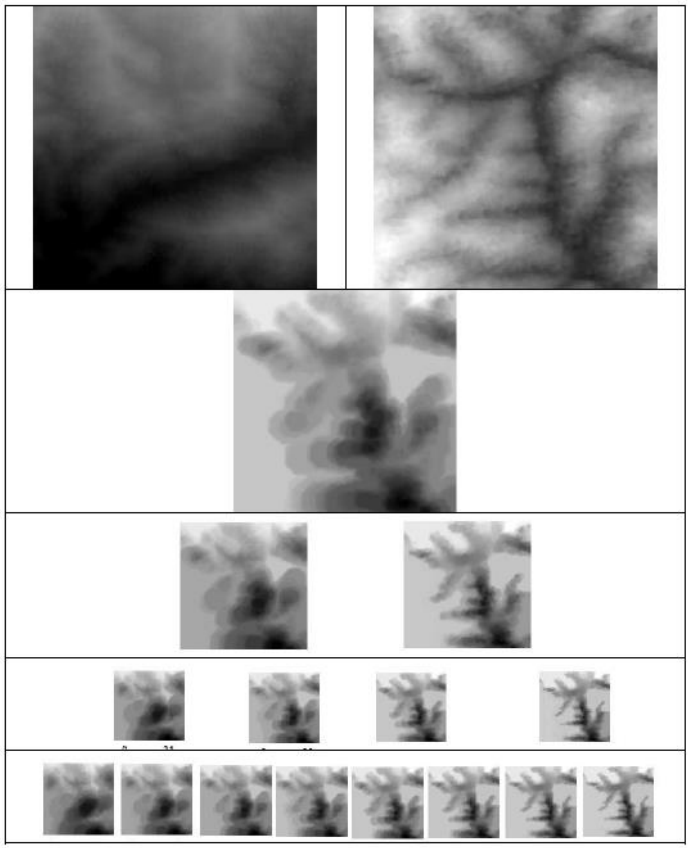

Source and Target DEMs

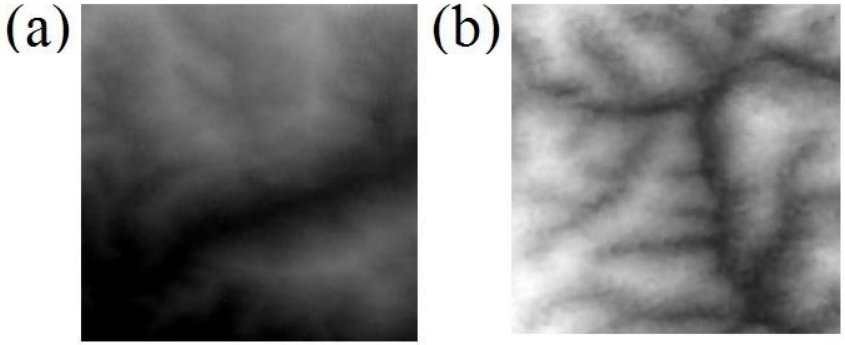

MORPHOLOGICAL MEDIANS

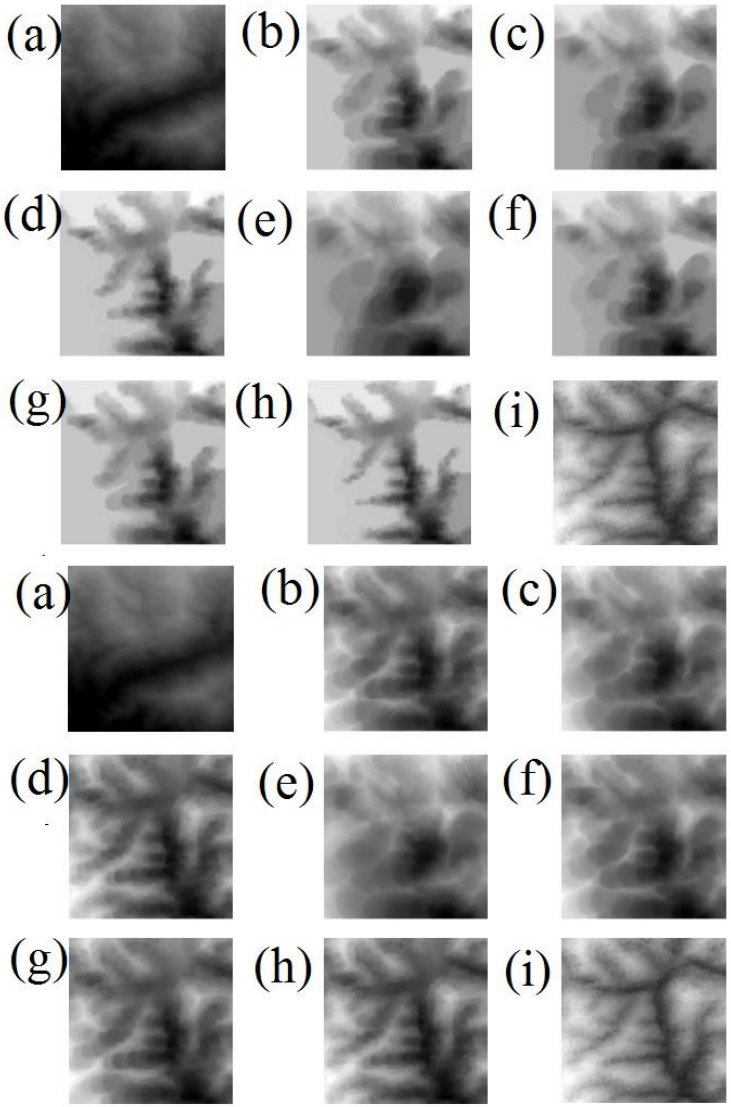

Morphing via Flat and a Non-Flat Structuring Elements

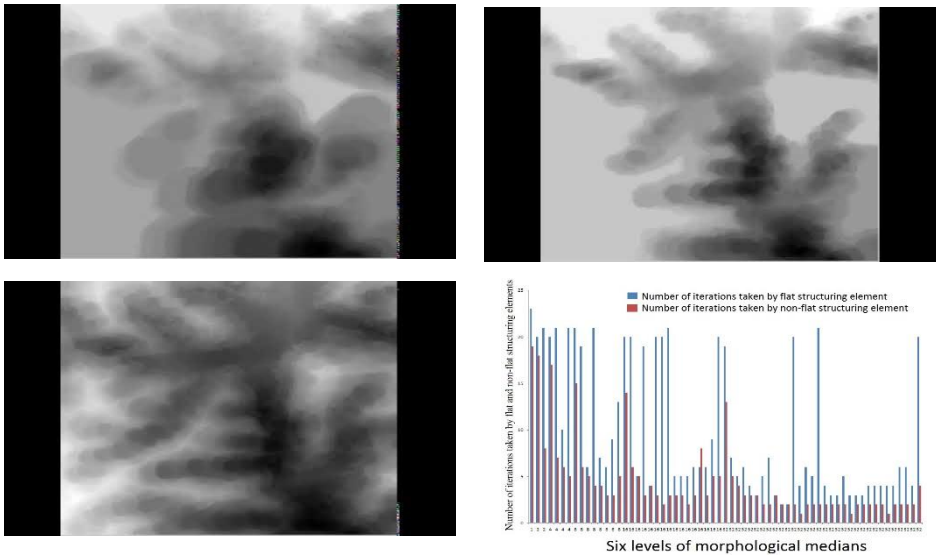

Morphing: Flat Vs Non-Flat

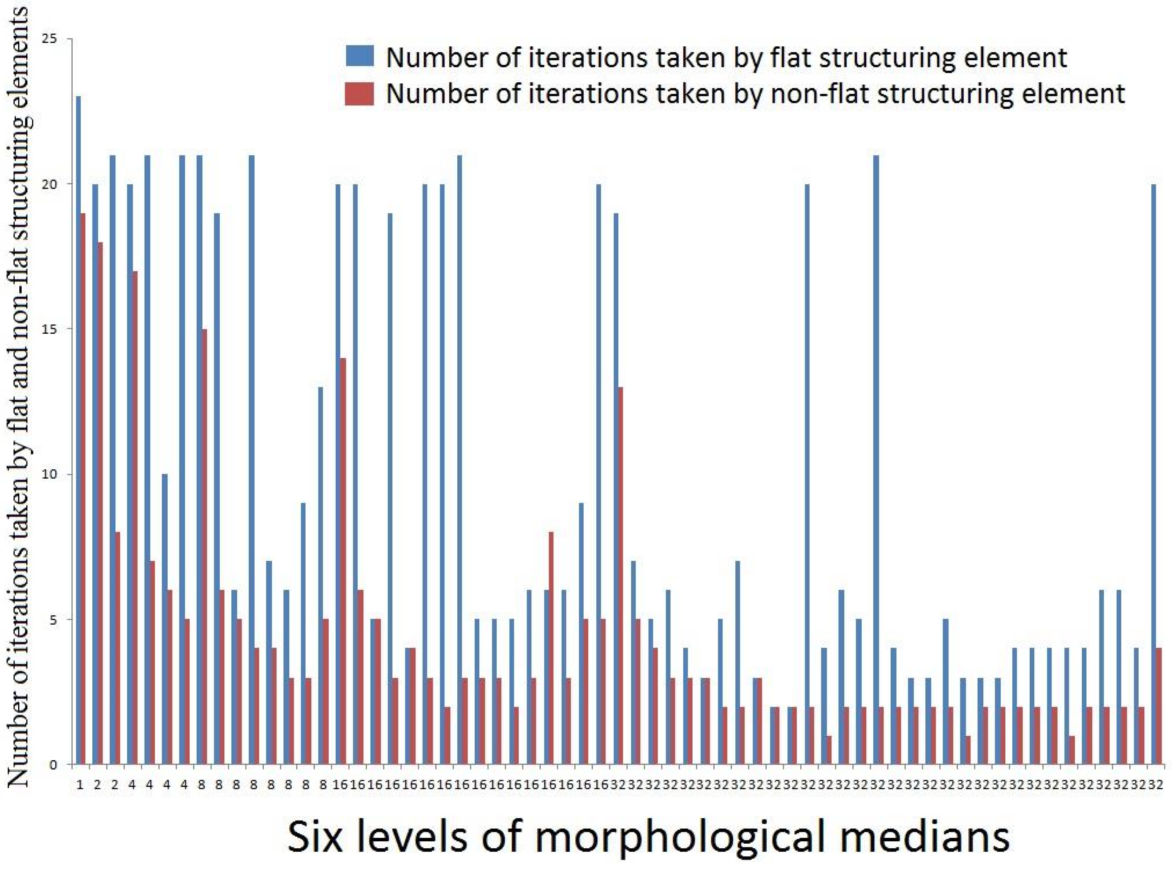

Watersheds (Zones of Influence) and Powerlaws

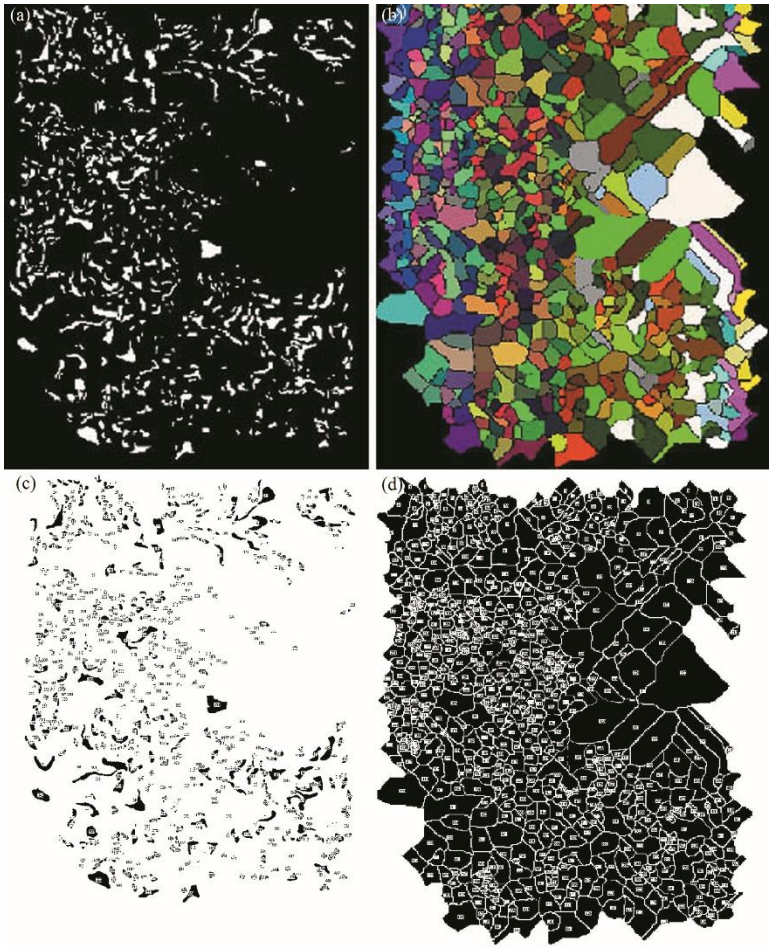

$$Z(A_i) = \bigcup_{n} \left(\delta^{n}_{\lambda_i}(A_i) \cap A \right) \setminus \bigcup_{\forall j} \left(\delta^{n}_{\lambda_{j \neq i}}(A_j) \cap A \right)$$

$$Z(A) = \left(\bigcup_{i} (Z(A_i)) \right)^{C}$$

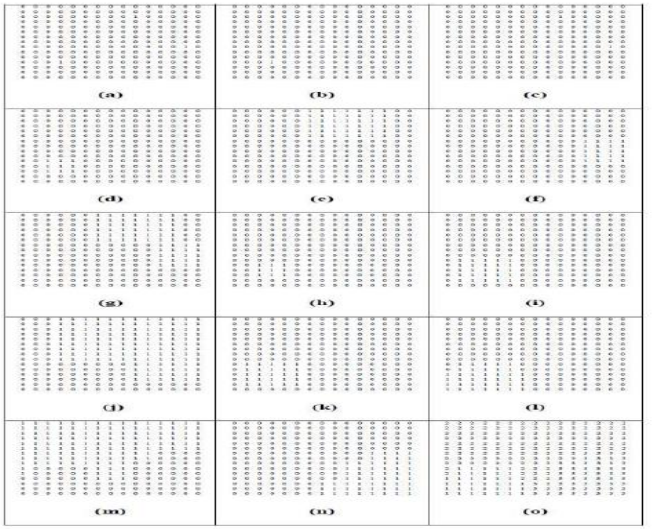

Fig. S1. (a) original map with three points (shown with 1s) for (A_1), (A_2), and (A_3), (b) i^{th} point $(A_i) = (A_i)$, (c) union of i^{th} points, $\bigcup_{\forall i} A_i = (A_1) \bigcup (A_2)$, (d) first cycle of dilation of i^{th} point by B (Square in shape) with the propagation speed of $\lambda = 1$, denoted by $\delta^{\lambda=1}(A_i)$, (e) first cycle of dilation of i^{th} point (A_2) by B with the propagation speed of $\lambda = 3$, $\delta^{\lambda=3}(A_2)$, (f) first cycle of dilation of i^{th} point (A_2) by B with the propagation speed of $\lambda = 2$, $\delta^{\lambda=2}(A_2)$, (g) union of $\delta^{\lambda=1}(A_1)$ and $\delta^{\lambda=3}(A_2)$, (h) $\delta^{\lambda=1}(A_1) \setminus \delta^{\lambda=3}(A_2) \bigcup \delta^{\lambda=3}(A_2)$, (i) $\delta^{\lambda=2}(A_3)$ (j) similarly for next iteration: $\delta^{\lambda=1}(A_1) \bigcup \delta^{\lambda=3}(A_2)$, (k) $\delta^{\lambda=1}(A_1) \setminus \delta^{\lambda=3}(A_2) \bigcup \delta^{\lambda=3}(A_2)$, (l) $Z(A_1) = \bigcup \left[\delta^{\lambda=1}(A_1) \setminus \delta^{\lambda=3}(A_2) \bigcup \delta^{\lambda=2}(A_3) \right]$, (m) similarly follow the steps from (b-l) by changing the i^{th} point from (A_1) to (A_2), and by treating (A_1) and (A_3) as i^{th} points; the $Z(A_2)$ is obtained, (n) obtained $Z(A_3)$, and (o) three zones $Z(A_1)$, $Z(A_2)$, and $Z(A_3)$ are shown with 1s, 2s, and 3s.

Point-to-Polygon Conversion

http://www.isibang.ac.in/~bsdsagar/AnimationOfPointPolygonConversion.wmv

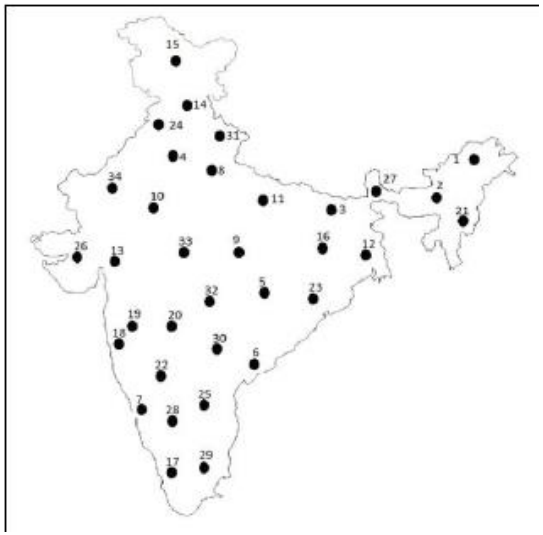

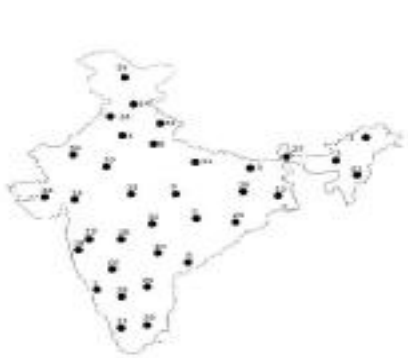

(a) (b)

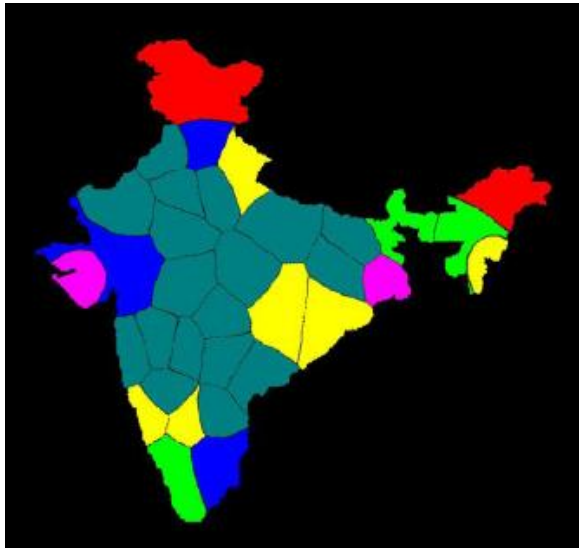

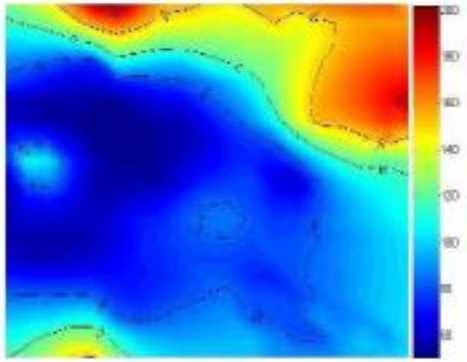

(c) (d)

Fig. 4. (a) 34 points (locations) of rain-gauge stations spread over India indexed ($A_1 - A_{34}$), (b) Rainfall zonal map generated by having various possible propagation speeds, and the variable strengths in terms of propagation speeds are given according to ranks shown in Table 1, (c) broader zones obtained after merging the zones (Fig. 4b) obtained with similar propagation speeds, and (d) kriged map generated for 34 gauge station data.

States as Basins, MSPs, SKIZ, WSKIZ & Cartograms

$$CZ(A_i) = \bigcup_n \left(\delta^n_{\lambda_i}(A_i^C) \cap A\right) \setminus \bigcup_{\forall j} \left(\delta^n_{\lambda_{j\neq i}}\left(A_j^C\right) \cap A\right) \quad (2)$$

$$CZ(A) = \left(\bigcup_i (CZ(A_i))\right)^C \quad (3)$$

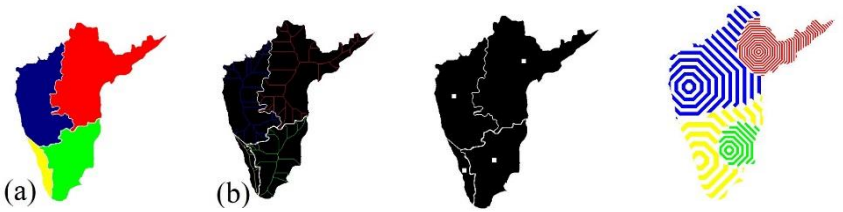

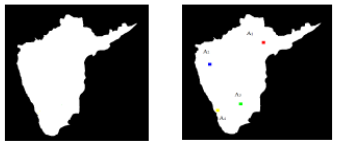

(a) (b)

Fig. 2. (a) region considered is south India, and (b) gauge-station locations (A_1, A_2, A_3, A_4).

(a) (b) (c) (d)

Fig. 3. The variable strengths (in terms of propagation speeds are given as (a) $A_2 > A_4 > A_1 > A_3$, (b) $A_2 > A_1 > A_3 > A_4$, (c) $A_1 > A_3 > A_2 > A_4$, and (d) $A_1 > A_4 > A_2 > A_3$.

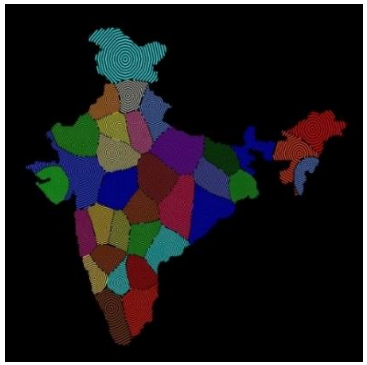

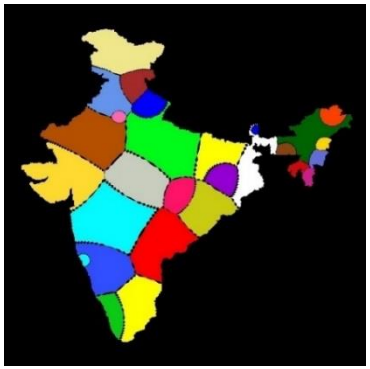

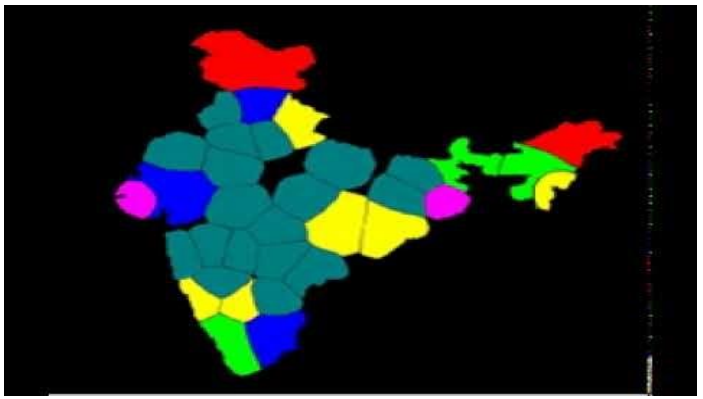

Overview

I. Digital Elevation Models (DEMs): An Important Source Data for Geoscientists

II. Mathematical Morphology: Notations, Equations, and Transformations

III. Mathematical Morphology in DEMs

- Skeletonization in DEMs and DEM Partitions
- Granulometries: Surficial roughness characterization/ quantification
- Geodesic Spectrum in Bottom Topography Studies
- Morphological Interpolations: Morphing of Source DEM into Target DEM
- Ranks for Pairs of Images; DEM Classification
- Morphological distances in spatial optimization and interaction modeling

IV. How the above studies could be integrated to better understand the surficial process dynamics?

III.V. Mathematical Morphology in Classification

I. Morphology in classification

II. Grouping of remotely sensed satellite data via rankings for pairs

Morphology in Classification

Jón Atli Benediktsson, Jón Aevar Palmason, and Johannes R. Sveinsson, Classification of Hyperspectral Data From Urban Areas Based on Extended Morphological Profiles, IEEE Transaction on Geoscience and Remote Sensing, v. 43, no. 3, p. 48-491, 2005.

Aditya Challa, Sravan Danda, B. S. Daya Sagar, and Laurent Najman, 2021, Triplet-Watershed for Hyperspectral Image Classification, IEEE Transactions on Geoscience and Remote Sensing, (In Press). DOI: 10.1109/TGRS.2021.3113721

Grouping of Remotely Sensed Satellite Data via Rankings for Pairs

B. S. Daya Sagar and Lim Sin Liang, 2015, Ranks for pairs of spatial fields via metric based on grayscale morphological distances, IEEE Transactions on Image Processing, v. 24, no. 3, p. 908-918, (DOI:10.1109/TIP.2015.2390135).

EQUATIONS

$$d\left(f^i, f^j\right) = \min\left\{n : A\left(f^i \vee f^j\right) < A\left(\left(f^i \wedge f^j\right) \oplus nB\right)\right\} \tag{6}$$

$$e\left(f^i, f^j\right) = \min\left\{n : A\left(\left(f^i \vee f^j\right) \ominus nB\right) < A\left(f^i \wedge f^j\right)\right\} \tag{7}$$

$$d^*\left(f^i, f^j\right) = \min\left\{n : \begin{pmatrix}\left(A\left(f^i \wedge f^j\right) \oplus nB\right) \\ = \left(A\left(f^i \wedge f^j\right) \oplus (n+1)B\right)\end{pmatrix} \ll A\left(f^i \vee f^j\right)\right\} \tag{8}$$

$$e^*\left(f^i, f^j\right) = \min\left\{n : \begin{pmatrix}\left(A\left(f^i \vee f^j\right) \ominus nB\right) \\ = \left(A\left(f^i \vee f^j\right) \ominus (n+1)B\right)\end{pmatrix} \ll A\left(f^i \wedge f^j\right)\right\} \tag{9}$$

III.V.I. Ranks for Pairs of Images: DEM Classification

EQUATIONS

$$R_{f^i f^j} = \left(\frac{A\left(f^i \wedge f^j\right)}{A\left(f^i \vee f^j\right)}\right)\left(\frac{\min\left(e\left(f^i, f^j\right), d\left(f^i, f^j\right)\right)}{\max\left(e\left(f^i, f^j\right), d\left(f^i, f^j\right)\right)}\right), \tag{22}$$

$$\begin{bmatrix} A\left(f^1 \wedge f^1\right) & A\left(f^2 \wedge f^1\right) & \cdots & A\left(f^N \wedge f^1\right) \\ A\left(f^1 \wedge f^2\right) & A\left(f^2 \wedge f^2\right) & \cdots & A\left(f^N \wedge f^2\right) \\ \vdots & \vdots & \ddots & \vdots \\ A\left(f^1 \wedge f^N\right) & A\left(f^2 \wedge f^N\right) & \cdots & A\left(f^N \wedge f^N\right) \end{bmatrix} \tag{14}$$

$$\begin{bmatrix} A\left(f^1 \vee f^1\right) & A\left(f^2 \vee f^1\right) & \cdots & A\left(f^N \vee f^1\right) \\ A\left(f^1 \vee f^2\right) & A\left(f^2 \vee f^2\right) & \cdots & A\left(f^N \vee f^2\right) \\ \vdots & \vdots & \ddots & \vdots \\ A\left(f^1 \vee f^N\right) & A\left(f^2 \vee f^N\right) & \cdots & A\left(f^N \vee f^N\right) \end{bmatrix} \tag{15}$$

$$\begin{bmatrix} d\left(f^1, f^1\right) & d\left(f^2, f^1\right) & \cdots & d\left(f^N, f^1\right) \\ d\left(f^1, f^2\right) & d\left(f^2, f^2\right) & \cdots & d\left(f^N, f^2\right) \\ \vdots & \vdots & \ddots & \vdots \\ d\left(f^1, f^N\right) & d\left(f^2, f^N\right) & \cdots & d\left(f^N, f^N\right) \end{bmatrix} \tag{17}$$

$$\begin{bmatrix} e\left(f^1, f^1\right) & e\left(f^2, f^1\right) & \cdots & e\left(f^N, f^1\right) \\ e\left(f^1, f^2\right) & e\left(f^2, f^2\right) & \cdots & e\left(f^N, f^2\right) \\ \vdots & \vdots & \ddots & \vdots \\ e\left(f^1, f^N\right) & e\left(f^2, f^N\right) & \cdots & e\left(f^N, f^N\right) \end{bmatrix} \tag{18}$$

$$\begin{bmatrix} R_{f^1,f^1} & R_{f^2,f^1} & \cdots & R_{f^N,f^1} \\ R_{f^1,f^2} & R_{f^2,f^2} & \cdots & R_{f^N,f^2} \\ \vdots & \vdots & \ddots & \vdots \\ R_{f^1,f^N} & R_{f^2,f^N} & \cdots & R_{f^N,f^N} \end{bmatrix} \tag{23}$$

From (23), one can rank the pair of spatial fields from most similar to the most dissimilar as (24).

$$R_{B;f^i,f^j} = \max_{\forall i}\left\{\max_j\left(R_{f^i,f^j}\right)\right\} \tag{24}$$

PROPERTIES

This ranking index satisfies the following conditions:

1) This ranking equation (24) provides symmetric results such that when designating the rank to a pair (f^i and f^j), exchanging the order of the spatial fields as f^j and f^i should not affect the results.
2) *Boundedness:* $R_{f^i f^j} \leq 1$, such that the upper bound serves as an indication of how the f^i and f^j are being perfectly identical.
3) *Unique Maximum:* $R_{f^i f^j} = 1 \Leftrightarrow f^i = f^j$. The perfect score is achieved if and only if the f^i and f^j being compared are identical.

Histogram Equalized Spatial Fields

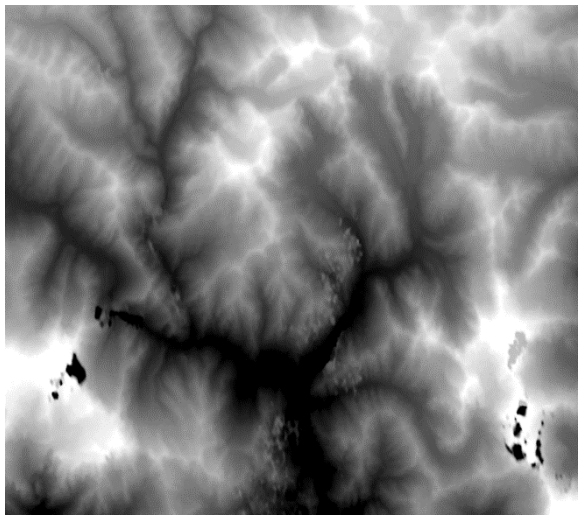

USGS SRTM Data

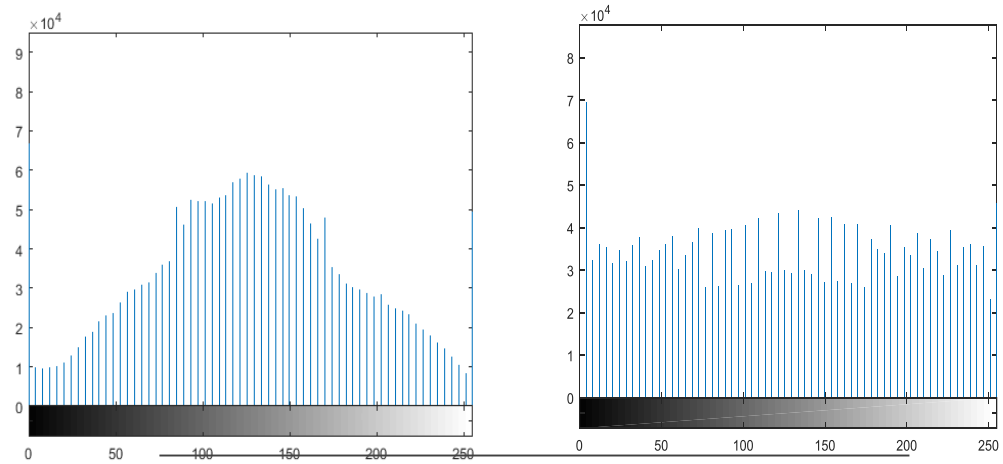

Segmentation into 4 equal halves

SRTM	F11	F12	F13	F14
F11	1	0.442	0.493	0.419
F12	0.442	1	0.329	0.150
F13	0.493	0.329	1	0.468
F14	0.419	0.150	0.468	1

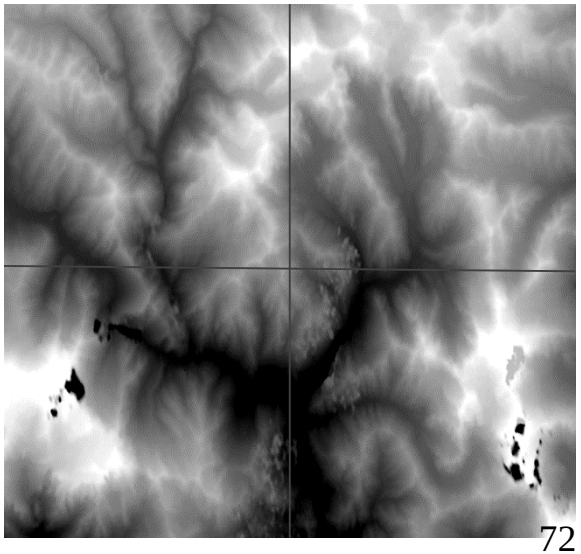

DIGITAL ELEVATION MODELS

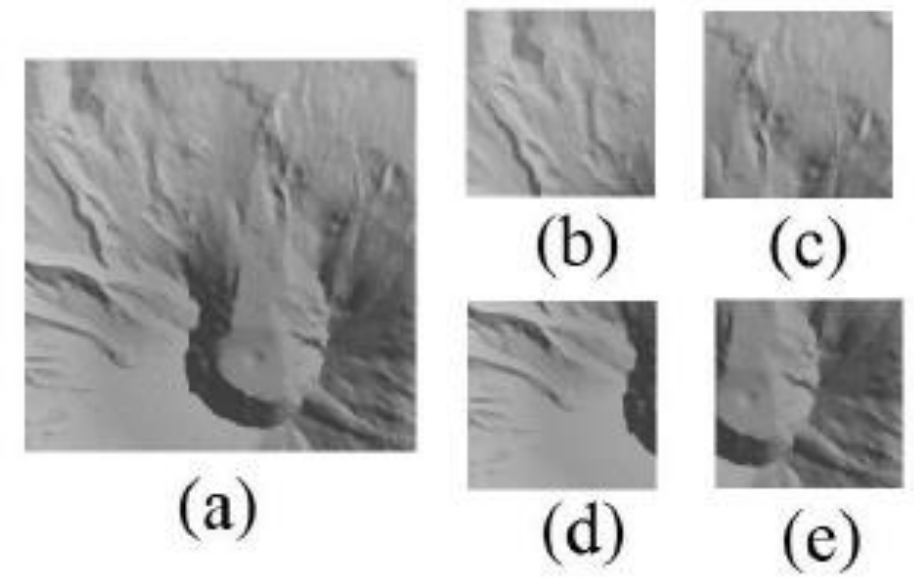

Fig. 7. (a) Digital Elevation Model of size 256×256 pixels depicting Mount St Helens, (b-e) four quadrants of size 128×128 pixels partitioned from DEM (Fig. 7a) include top-left $\left(f^1\right)$, top-right $\left(f^2\right)$, bottom-left $\left(f^3\right)$, and bottom-right $\left(f^4\right)$ portions.

BEST-PAIRS OF DEMs

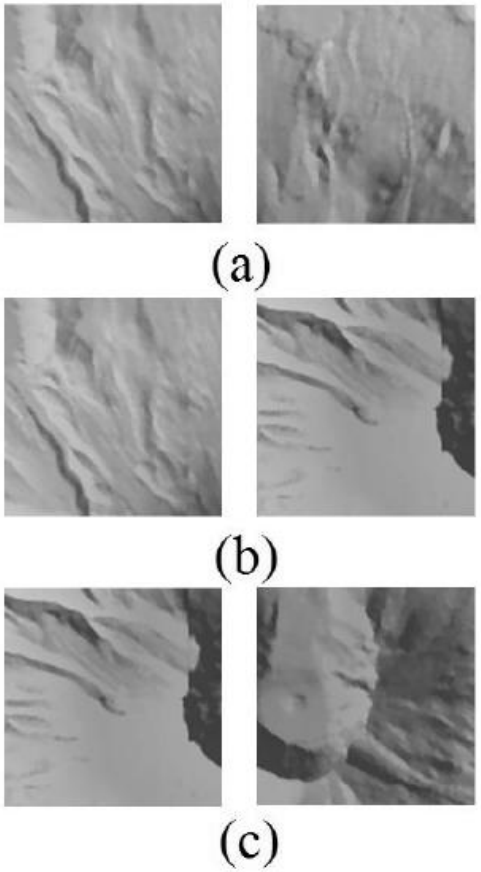

Fig. 8. Three best ranked pairs of spatial elevation fields shown in Fig. 7b-e (a) (f^1, f^2), (b) (f^1, f^3), and (c) (f^3, f^4).

SIMILARITY INDEXES COMPUTED FOR ALL POSSIBLE PAIRS OF SPATIAL ELEVATION FIELDS

	f^1	f^2	f^3	f^4
f^1	1	0.8514	0.6505	0.5694
f^2	0.8514	1	0.5456	0.6120
f^3	0.6505	0.5456	1	0.6505
f^4	0.5694	0.6120	0.6505	1

Overview

I. Digital Elevation Models (DEMs): An Important Source Data for Geoscientists

II. Mathematical Morphology: Notations, Equations, and Transformations

III. Mathematical Morphology in DEMs

- Skeletonization in DEMs and DEM Partitions
- Granulometries: Surficial roughness characterization/ quantification
- Geodesic Spectrum in Bottom Topography Studies
- Morphological Interpolations: Morphing of Source DEM into Target DEM
- Ranks for Pairs of Images; DEM Classification
- Morphological distances in spatial optimization and interaction modeling

IV. How the above studies could be integrated to better understand the surficial process dynamics?

III.VI. Quantitative Spatial Resoning

Strategic Set Identification

- Spatial Entities (e.g.: water bodies, zones of influence, geomorphic basins, and urban features of the specific thematic maps) can be well identified/ mapped from Digital Elevation Models generated from high resolution remotely sensed data.
- Understanding the organization of these spatial entities is an important aspect from the point of '**Spatial Reasoning**'.

Spatially Significant Zones

- Spatially Significant Zone (SSZ) can be defined as **"a zone from which it is easy to reach all of its neighbouring zones".**
- Cluster of spatial entities (zones) can be treated as a **'Spatial System' (e.g.:** Geomorphological basin (cluster of sub-basins) consists of sub-basins (zones), and sub-basins consist of still minor sub-basins, and so on).

Spatial System - SSZ

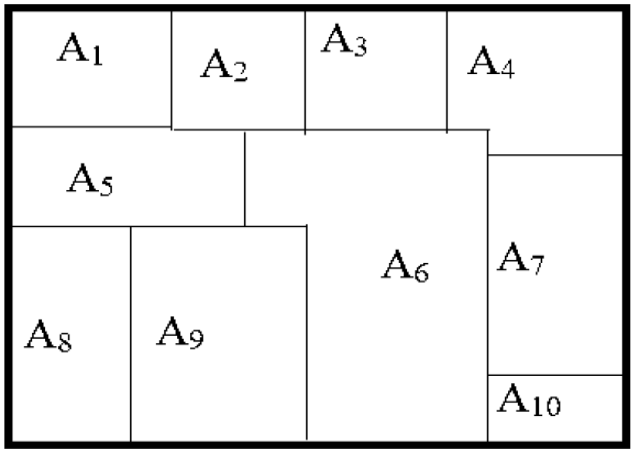

Fig: A 2-D representation of a spatial system with 10 zones.

For a geometric basin (Ai), if A1 is considered as an origin zone, then all the other zones (A2-A10) are treated as destination zones.

$$A_1, A_2, A_3, \cdots, A_N$$

$$A = \bigcup_{i=1}^{N} A_i$$

$$A_i \cap A_j = \varnothing$$

I

II

$$A_i \cap \left(\bigcup_{\substack{j=1 \\ j \neq i}}^{N} A_j \right) = \varnothing, \forall i, j = 1 - N$$

III

$$(A_i \oplus B) \cap \left(\bigcup_{\substack{j=1 \\ j \neq i}}^{N} A_j \right) = \left(\left(\left(\bigcup_{\substack{j=1 \\ j \neq i}}^{N} A_j \right) \oplus B \right) \cap A_i \right) \neq \varnothing$$

- The relations I & II would be satisfied for the cases of water bodies, nodes, point-specific data.
- Relation III will be satisfied, if all the zones of a cluster are in contiguous form.

Iterative Dilation Distances

Let non-empty, disjoint compact zones Ai and Aj be the original and destination zones. (**Ai < Aj**)

- The distance from Ai to Aj represented by:

$$d\left(A_{ji}\right) = \min_{i \neq j}\left(n : A_i \subseteq \left(A_j \oplus nB\right)\right)$$

- The distance between Aj and Ai represented by:

$$d\left(A_{ij}\right) = \min_{i \neq j}\left(n : A_j \subseteq \left(A_i \oplus nB\right)\right)$$

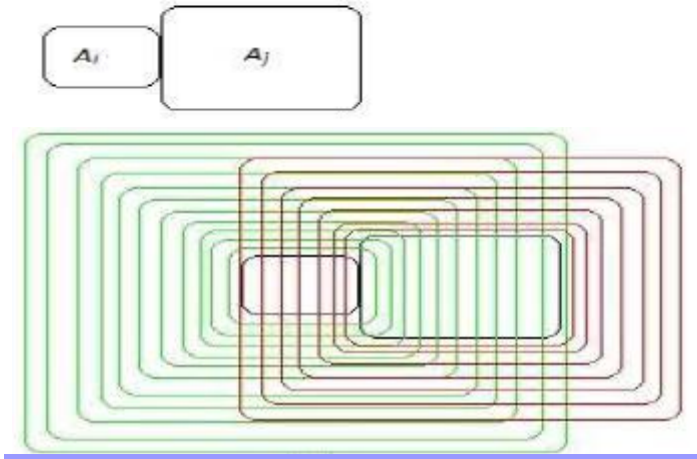

dilation distances $d\left(A_{ij}\right) = 11$, and $d\left(A_{ji}\right) = 7$, and $\rho\left(A_{ij}\right) = 7$

The following conditions will be satisfied, iff both '**Ai**' & '**Aj**' possess identical size, shape & orientation.

$$d\left(A_{ij}\right) = d\left(A_{ji}\right)$$

$$d\left(A_{ii}\right) = 0,\quad d\left(A_{ij}\right) \neq d\left(A_{ji}\right)$$

SSI & NSSI of a Zone

- Normalized Spatial Significance Index (NSSI) that ranges between **0** and **1** takes form of:

$$SSI = \min_{\forall i}\left(d_{\max}\left(A_{ij}\right)\right)$$

$$NSSI = \left(\frac{\min\limits_{\forall i}\left(d_{\max}\left(A_{ij}\right)\right)}{\max\limits_{\forall i}\left(d_{\max}\left(A_{ij}\right)\right)}\right)$$

- If the zones of a cluster are **identical**, then:

$$\min_{\forall i}\left(d_{\max}\left(A_{ii}\right)\right) \quad \min_{\forall j}\left(d_{\max}\left(A_{ji}\right)\right)$$

- If the zones of a cluster are **dissimilar**, then:

$$\min_{\forall i}\left(d_{\max}\left(A_{ii}\right)\right) \quad \min_{\forall j}\left(d_{\max}\left(A_{ji}\right)\right)$$

- When all the zones in a cluster are similar both in terms of size & shape, the following relationship holds **good**.

$$\left(\frac{\min\limits_{\forall i}\left(d_{\max}\left(A_{ij}\right)\right)}{\max\limits_{\forall i}\left(d_{\max}\left(A_{ij}\right)\right)}\right) = \left(\frac{\min\limits_{\forall j}\left(d_{\max}\left(A_{ji}\right)\right)}{\max\limits_{\forall j}\left(d_{\max}\left(A_{ji}\right)\right)}\right)$$

SSI-Cluster of Zones of Water Body Influence

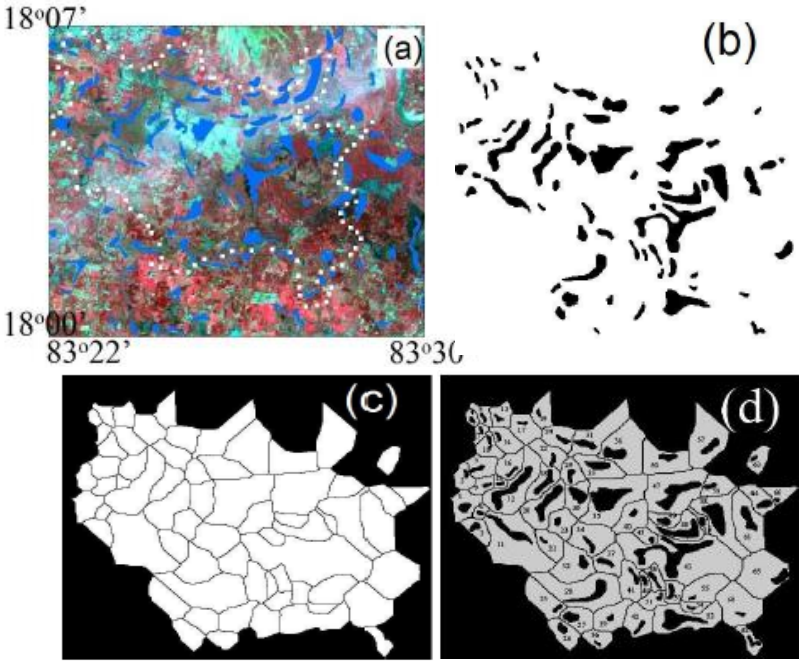

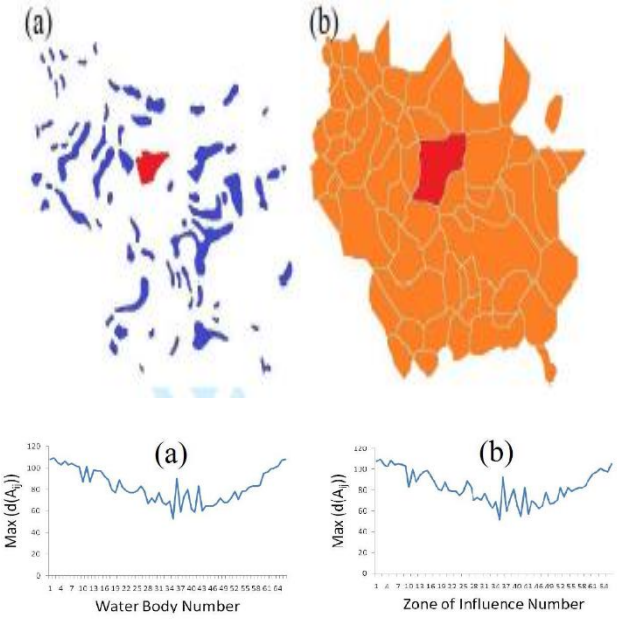

a. LISS-III input image, b. **66 e**xtracted water bodies from RS data, c. Corresponding Zones of influence, water bodies. d. Water bodies and zones with labeling.

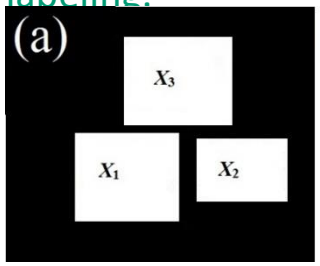

(b)

	X_1	X_2	X_3	$d_{max}(X_{ji})$
X_1	0	6	7	7
X_2	5	0	4	5
X_3	7	5	0	7
$d_{max}(X_{ij})$	7	6	7	

TABLE I. SSI OF TOP FIVE WATER BODIES AND ZONES

RANK	WATER BODY (W) LABEL	D-DIST	ZONE (Z) LABEL	D-DIST	NSSI (W)	NSSI (Z)
1	35	53	35	52	0.48	0.47
2	41	59	41	55	0.54	0.50
3	43	59	43	57	0.54	0.51
4	49	60	37	60	0.55	0.54
5	46	62	46	62	0.56	0.56

Dilation-Distance Based Directional Spatial Relationship and Orientation Detection: Animation

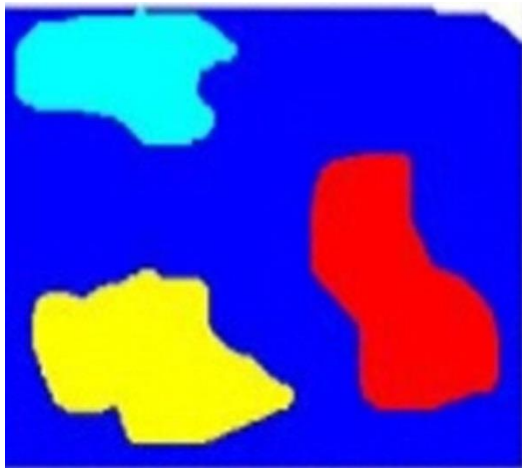

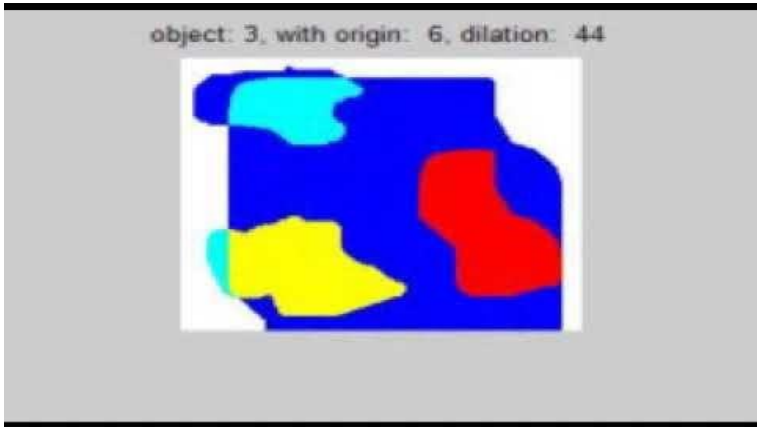

Spatial Interactions

EQUATIONS: SPATIAL INTERACTION

$$X_i \cap \left(\bigcup_{\substack{j=1 \\ j \neq i}}^{N} X_j \right) = \varnothing .$$

$$FX_{ij} = G \frac{mX_i mX_j}{\left(dX_{ij}\right)^2}$$

$$\left(\varphi X_i\right) = \left(\frac{\max_{\forall j}\left(d\left(X_{ij}\right)\right)}{\max_{\forall i}\left(\max_{\forall j}\left(d\left(X_{ij}\right)\right)\right)} \right)$$

$$d\left(X_{ij}\right) = \begin{bmatrix} & X_1 & X_2 & \cdots & X_N \\ X_1 & d\left(X_{11}\right) & d\left(X_{21}\right) & \cdots & d\left(X_{N1}\right) \\ X_2 & d\left(X_{12}\right) & d\left(X_{22}\right) & \cdots & d\left(X_{N2}\right) \\ \vdots & \vdots & \vdots & \ddots & \vdots \\ X_N & d\left(X_{1N}\right) & d\left(X_{2N}\right) & \cdots & d\left(X_{NN}\right) \end{bmatrix} \quad (9)$$

$$\left(\varphi X_i \varphi X_j\right) = \begin{bmatrix} & \varphi X_1 & \varphi X_2 & \cdots & \varphi X_N \\ \varphi X_1 & \left(\varphi X_1 \varphi X_1\right) & \left(\varphi X_2 \varphi X_1\right) & \cdots & \left(\varphi X_N \varphi X_1\right) \\ \varphi X_2 & \left(\varphi X_1 \varphi X_2\right) & \left(\varphi X_2 \varphi X_2\right) & \cdots & \left(\varphi X_N \varphi X_2\right) \\ \vdots & \vdots & \vdots & \ddots & \vdots \\ \varphi X_N & \left(\varphi X_1 \varphi X_N\right) & \left(\varphi X_2 \varphi X_N\right) & \cdots & \left(\varphi X_N \varphi X_N\right) \end{bmatrix} \quad (10)$$

$$\left(mX_i mX_j\right) = \begin{bmatrix} & mX_1 & mX_2 & \cdots & mX_N \\ mX_1 & \left(mX_1 mX_1\right) & \left(mX_2 mX_1\right) & \cdots & \left(mX_N mX_1\right) \\ mX_2 & \left(mX_1 mX_2\right) & \left(mX_2 mX_2\right) & \cdots & \left(mX_N mX_2\right) \\ \vdots & \vdots & \vdots & \ddots & \vdots \\ mX_N & \left(mX_1 mX_N\right) & \left(mX_2 \varphi mX_N\right) & \cdots & \left(mX_N mX_N\right) \end{bmatrix} \quad (11)$$

Level of interaction matrix is

$$F\left(X_{ij}\right) = \begin{bmatrix} & X_1 & X_2 & \cdots & X_N \\ X_1 & F\left(X_{11}\right) = \frac{\left(mX_1 mX_1\right)}{\left(d\left(X_{11}\right)\right)^2 \left(\varphi X_1 \varphi X_1\right)} & F\left(X_{21}\right) = \frac{\left(mX_2 mX_1\right)}{\left(d\left(X_{21}\right)\right)^2 \left(\varphi X_2 \varphi X_1\right)} & \cdots & F\left(X_{N1}\right) = \frac{\left(mX_N mX_1\right)}{\left(d\left(X_{N1}\right)\right)^2 \left(\varphi X_N \varphi X_1\right)} \\ X_2 & F\left(X_{12}\right) = \frac{\left(mX_1 mX_2\right)}{\left(d\left(X_{12}\right)\right)^2 \left(\varphi X_1 \varphi X_2\right)} & F\left(X_{22}\right) = \frac{\left(mX_2 mX_2\right)}{\left(d\left(X_{22}\right)\right)^2 \left(\varphi X_2 \varphi X_2\right)} & \cdots & F\left(X_{N2}\right) = \frac{\left(mX_N mX_2\right)}{\left(d\left(X_{N2}\right)\right)^2 \left(\varphi X_N \varphi X_2\right)} \\ \vdots & \vdots & \vdots & \ddots & \vdots \\ X_N & F\left(X_{1N}\right) = \frac{\left(mX_1 mX_N\right)}{\left(d\left(X_{1N}\right)\right)^2 \left(\varphi X_1 \varphi X_N\right)} & F\left(X_{2N}\right) = \frac{\left(mX_2 mX_N\right)}{\left(d\left(X_{2N}\right)\right)^2 \left(\varphi X_2 \varphi X_N\right)} & \cdots & F\left(X_{NN}\right) = \frac{\left(mX_N mX_N\right)}{\left(d\left(X_{NN}\right)\right)^2 \left(\varphi X_N \varphi X_N\right)} \end{bmatrix} \quad (12)$$

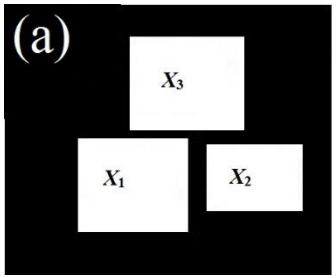

(b)

	X_1	X_2	X_3	$d_{max}(X_{ji})$
X_1	0	6	7	7
X_2	5	0	4	5
X_3	7	5	0	7
$d_{max}(X_{ij})$	7	6	7	

$$F\left(X_{ij}\right) = \frac{\left(mX_i mX_j\right)}{\left(d\left(X_{ij}\right)\right)^2 \left(\varphi X_i \varphi X_j\right)}$$

$$F\left(X_{ji}\right) = \frac{\left(mX_j mX_i\right)}{\left(d\left(X_{ji}\right)\right)^2 \left(\varphi X_j \varphi X_i\right)}$$

BEST PAIRS: FORCE OF INTERACTIONS

$$BX_i = \max_{\forall i,\forall j}\left\{\sum_j F(X_{ij}), \sum_i F(X_{ji})\right\} = \max\left\{\max_{\forall i}\left(\sum_j F(X_{ij})\right), \max_j\left(\sum_i F(X_{ji})\right)\right\} \quad .(13)$$

$$BX_{ij} = \max_{\forall i}\left(\max_{\forall j}\left(F\left(X_{ij}\right)\right)\right) \quad (14a)$$

$$BX_{ji} = \max_{\forall j}\left(\max_{\forall i}\left(F\left(X_{ji}\right)\right)\right)$$

$$\sum_i\left(\sum_j FX_{ij} = \frac{\sum_j mX_i mX_j}{\sum_j\left(dX_{ij}\right)^2 \sum_j\left(\varphi X_i \varphi X_j\right)}\right) \quad (16)$$

$$\sum_j\left(\sum_i FX_{ji} = \frac{\sum_i mX_j mX_i}{\sum_i\left(dX_{ji}\right)^2 \sum_i\left(\varphi X_j \varphi X_i\right)}\right) \quad (17)$$

Variable-Specific Classification of Zones, Pairs of Zones, and Clusters of a Spatial System via Modified Gravity Model

Figure 1 (a) Asian continent--Spatial system, (b) India-a cluster of the spatial system shown in (a), and (c) States of India-zones of the cluster shown in (b), which is a map of India (cluster of a spatial system) with 28 states (zones)—indexed according to alphabetical order—Andhra Pradesh (X_1), Arunachal Pradesh (X_2), Assam (X_3), Bihar (X_4), Chhattisgarh (X_5), Goa (X_6), Gujarat (X_7), Haryana (X_8), Himachal Pradesh (X_9), Jammu & Kashmir (X_{10}), Jarkhand (X_{11}), Karnataka (X_{12}), Kerala (X_{13}), Madhya Pradesh (X_{14}), Maharashtra (X_{15}), Manipur (X_{16}), Meghalaya (X_{17}), Mizoram (X_{18}), Nagaland (X_{19}), Orissa (X_{20}), Punjab (X_{21}), Rajasthan (X_{22}), Sikkim (X_{23}), Tamilnadu (X_{24}), Tripura (X_{25}), Uttarapradesh (X_{26}), Uttarakhand (X_{27}), West Bengal (X_{28}).

Figure 5. India map with each state designated with a rank with respect to four different parameters. (a) φX_i, (b) $\max_i\left(\sum_j FX_{ij}\right)$, (c) $\max_j\left(\sum_i FX_{ji}\right)$, and (d) $\max\left(\max_i\left(\sum_j FX_{ij}\right), \max_j\left(\sum_i FX_{ji}\right)\right)$

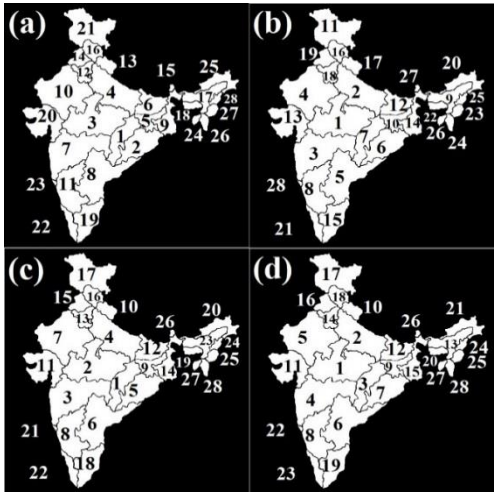

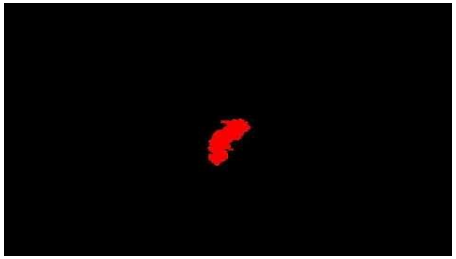

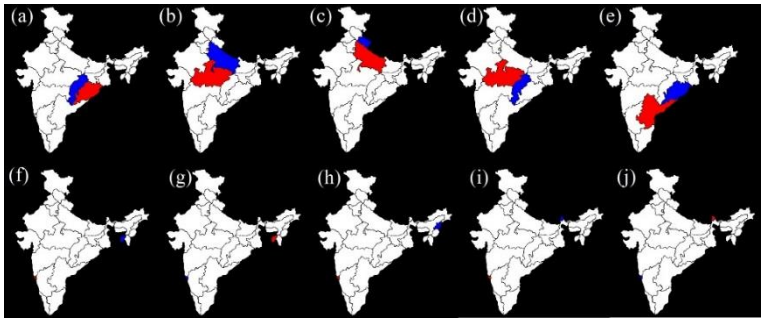

Figure 6. Five best pairs exhibited the high levels of interactions (a) $X_{20,5}$, (b) $X_{14,26}$, (c) $X_{26,27}$, (d) $X_{14,5}$, and (e) $X_{1,20}$. Five pairs exhibited the least levels of interactions (f) $X_{6,25}$, (g) $X_{25,6}$, (h) $X_{6,19}$, (i) $X_{6,23}$, and (j) $X_{23,6}$. Animation of the 756 successive interacting pairs can be seen at http://www.isibang.ac.in/~bsdsagar/MGM-Spatial-Interaction.avi.

B. S. Daya Sagar, Variable-Specific classification of zones, pairs of zones, and clusters of a spatial system via modified gravity model, *IEEE Transactions on Emerging Topics in Computing*, v.7, no. 2, p. 230-241, 2019.

Digital Elevation Model (DEM) is an Engineering Marvel: An important source of data for geoscientists

"Mathematical Morphology is an area of geoscience that most people don't realize will literally change the way they look at Earth!"

Mathematical Morphology: A Robust Mathematical Theory That Needs More Attention By Geoscience and Remote Sensing Communities

Some Special Issue of Journals and/or Books

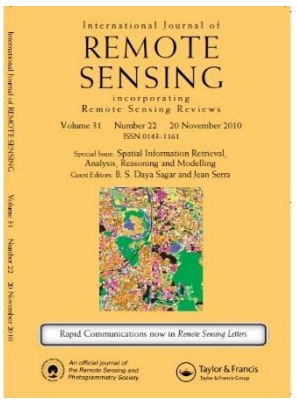

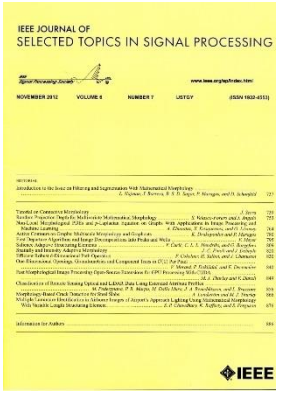

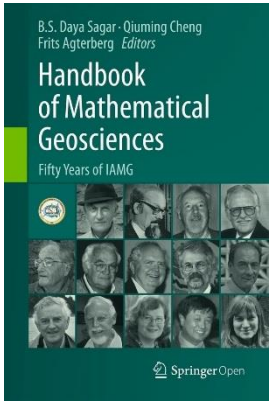

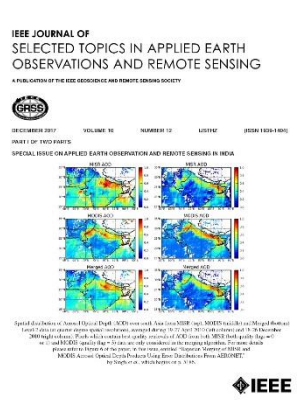

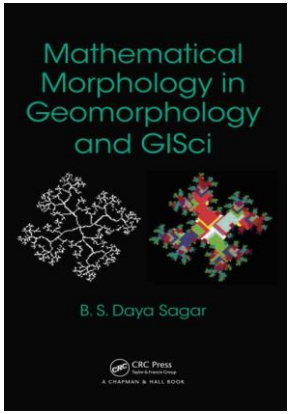

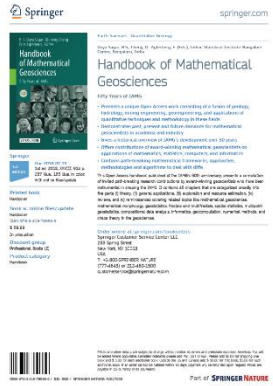

My Lectures on YouTube






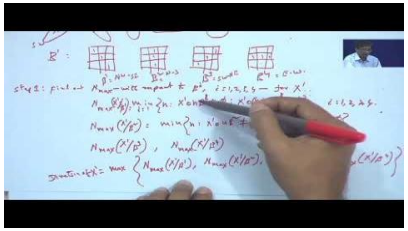


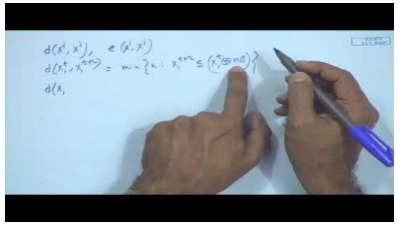
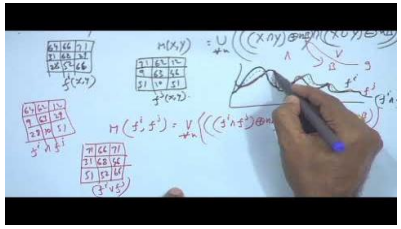

1. MM in Spatial Geodata Sciences
2. Binary Morphology
3. Binary and Grayscale Morphology
4. Grayscale MM, SKIZ, Interpolations
5. Interpolation and Cartogarms
6. Binary Granulometries
7. Directional and Grayscale Granulometries
8. Fractals and MSD
9. Morphological Distances
10. Morphing and Morphological Interpolations
11. Grayscale Morphological Interpolations

Call for Papers

http://www.grss-ieee.org/wp-content/uploads/2019/11/Call_for_Paper_MMRSG.pdf

CALL FOR PAPERS

IEEE Journal of Selected Topics in Applied Earth Observations and Remote Sensing
Special Issue on "Mathematical Morphology in Remote Sensing and Geoscience"

Historically, mathematical morphology was the first consistent non-linear image analysis theory, which from the very start included not only theoretical results but also many practical aspects. Mathematical morphology is capable of handling the most varied image types, in a way that is often subtle yet efficient. It can also be used to process general graphs, surfaces, implicit and explicit volumes, manifolds, time or spectral series, in both deterministic and stochastic contexts. In the last five years, connected signal representations and connected operators have emerged as tools for segmentation and filtering, leading to extremely versatile techniques for solving problems in a variety of domains including information science, geoscience, and image and signal analysis and processing. The application of mathematical morphology in processing and analysis of remotely sensed spatial data acquired at multi-spatial-spectral-temporal scales and by-products such as Digital Elevation Model (DEM) and thematic information in map forms has shown significant success in the last two decades. From data acquisition to the level of making theme-specific predictions, there exists several phases that include feature extraction (information retrieval), information analysis/characterization, information reasoning, spatio-temporal modelling and visualization. Relatively, numerous approaches/frameworks/schemes/ algorithms are available to address information retrieval when compare to those approaches available to address the rest of the topics. With the availability of data across various spatial/spectral/temporal resolutions, besides information extraction, other topics like pattern retrieval, pattern analysis, spatial reasoning, and simulation and modeling of spatiotemporal behaviors of several terrestrial phenomena and processes also need to be given emphasis. This special issue intends to bring high quality papers on theory and applications of mathematical morphology and scaling theories in addressing aforementioned intertwined topics.

The broad topics include (but are not limited to):

- Theory and applications of classical and modern mathematical morphology
- Mathematical morphology in color spaces
- Advances in filtering and segmentation and applications in remotely sensed data processing and analysis.
- Feature-based classification and clustering
- Morphological neural networks
- Stochastic geometry for deep learning
- Mathematical morphology in terrestrial pattern retrieval, terrestrial pattern analysis, quantitative spatial reasoning, geo-modelling, simulation and visualization, morphological interpolations and extrapolations
- Mathematical morphology in processing and analysis of Digital Elevation Models (DEMs)
- Applications of classical and modern mathematical morphology: Hyperspectral image analysis; 3-D object retrieval, stereoscopic image superpositions; texture hierarchical segmentation; stereoscopic image superpositions; cartographic images with emphasis on remote sensing, geoscience and information mining.

Schedule
October 1, 2020 Submission system opening
March 31, 2021 Submission system closing

Format
All submissions will be peer reviewed according to the IEEE Geoscience and Remote Sensing Society guidelines. Submitted articles should not have been published or be under review elsewhere. Submit your manuscript on http://mc.manuscriptcentral.com/jstars, using the Manuscript Central interface and select the "Mathematical Morphology" special issue manuscript type. Prospective authors should consult the site https://ieeexplore.ieee.org/stamp/stamp.jsp?tp=&arnumber=8855039 for guidelines and information on paper submission. All submissions must be formatted using the IEEE standard format (double column, single spaced). Please visit http://www.ieee.org/publications_standards/publications/authors/author_templates.html to download a template for transactions. Please note that as of Jan. 1, 2020, IEEE J-STARS will become a fully open-access journal charging a flat publication fee $1,250 per paper.

Guest Editors

B. S. Daya Sagar	Indian Statistical Institute – Bangalore Centre, India (bsdsagar@isibang.ac.in)
Jón Atli Benediktsson	University of Iceland, Iceland (benedikt@hi.is)
Lorenzo Bruzzone	University of Trento, Italy (lorenzo.bruzzone@unitn.it)
Jocelyn Chanussot	Grenoble Institute of Technology, France (jocelyn.chanussot@gipsa-lab.grenoble-inp.fr)

A Quick Recap…

- Essential ingredients to develop any model that leads to behavioral predictions are:
  - Retrieval of information
  - Quantitative information analysis
  - Quantitative information reasoning
  - Simulation and modeling of spatio-temporal behavior (*attractor* construction!)

Overview

I. Digital Elevation Models (DEMs): An Important Source Data for Geoscientists

II. Mathematical Morphology: Notations, Equations, and Transformations

III. Mathematical Morphology in DEMs

- Skeletonization in DEMs and DEM Partitions
- Granulometries: Surficial roughness characterization/ quantification
- Geodesic Spectrum in Bottom Topography Studies
- Morphological Interpolations: Morphing of Source DEM into Target DEM
- Ranks for Pairs of Images; DEM Classification
- Morphological distances in spatial optimization and interaction modeling

IV. How the above studies could be integrated to better understand the surficial process dynamics?

What is the use of these studies?

- With all these algorithms developed and/or developed to derive geometrically and topologically relevant information, can we make use of this information gathered across time instances to better understand (i) spatiotemporal behavior of terrestrial phenomena and (ii) dynamical behavior of terrestrial processes? This would be an Open challenge.

Attractors in Predictions

- Data and Information retrieved corresponding to systems with simple behaviors can be represented in the form of ***simple attractors***
- Data and Information retrieved corresponding to systems with strange behaviors can be represented in the form of ***strange attractors***
- ***Simple Attractors*** **possess low dimensionality, whereas** ***Strange Attractors*** **possess high dimensionality**
- **The predicting predictability of the systems with low dimensional attractors is rather straightforward.**
- **The predicting predictability of the systems with high dimensional attractors is complex.**

BIG Question(s)

- Do we have information thus retrieved precisely from DATA (whether Small or Big) that leads to construction of system-specific *attractor*?
- How big is the data that we require to construct such an attractor? An ad hoc answer is another question: What is the system that we are targeting?
- Can we categorize the systems as ‘soft’ and ‘hard’.
    - Soft – *simple attractor* – prediction possible
    - Hard – *strange attractor* – prediction (locally) is possible

Examples of Attractors: Toy Models

Numerical Data

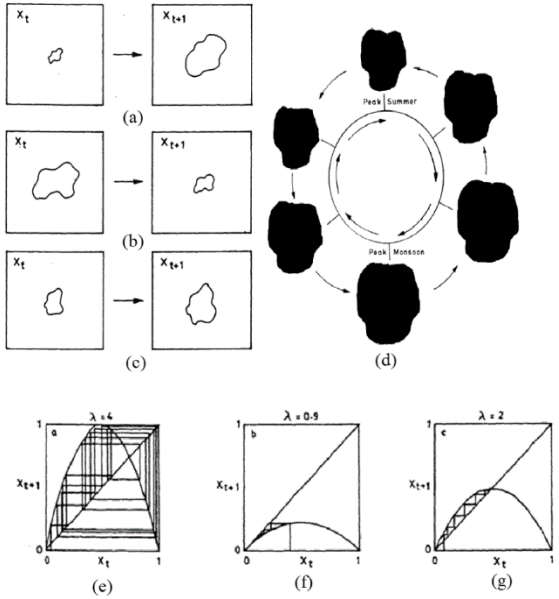

Attractors

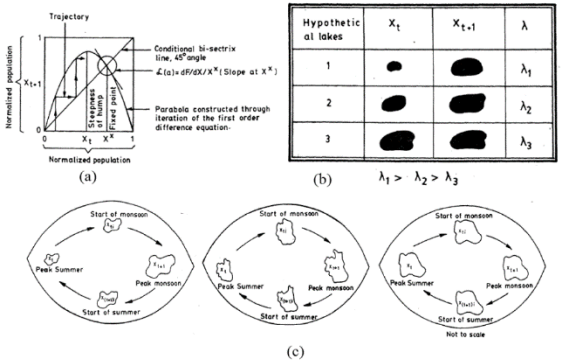

Behavior of Lakes

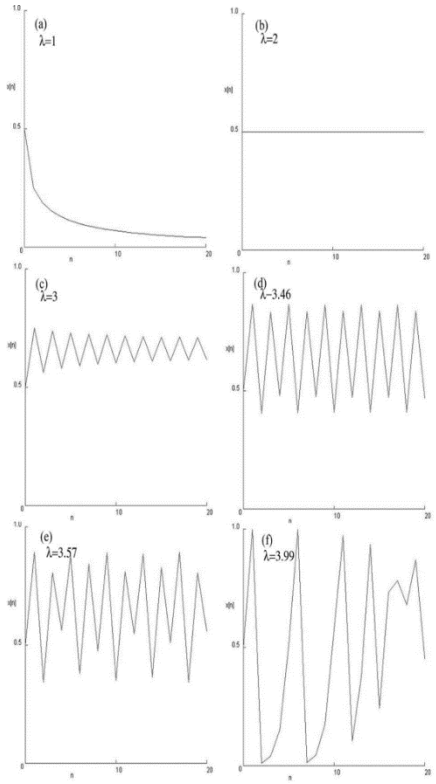

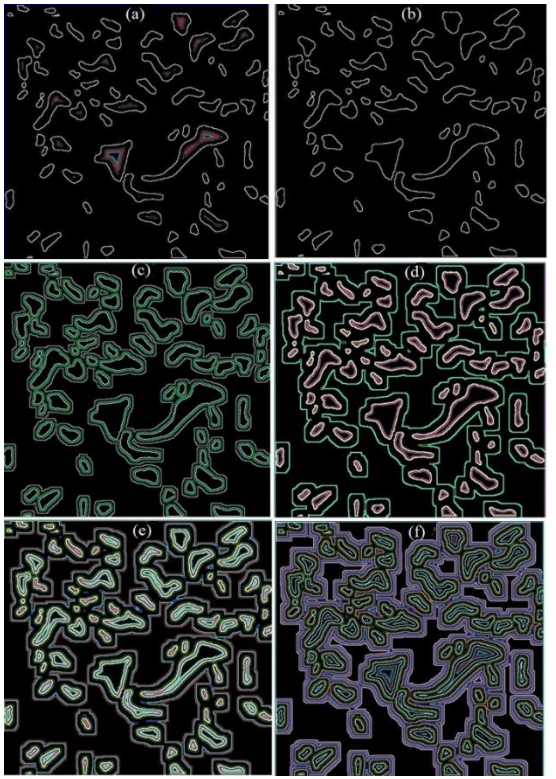

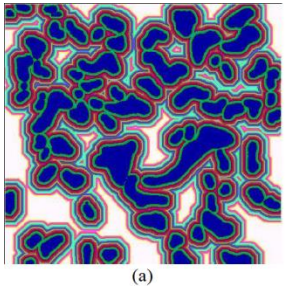

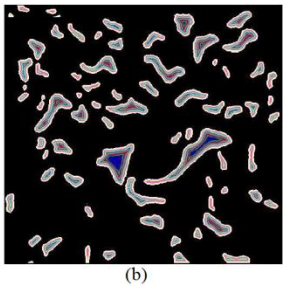

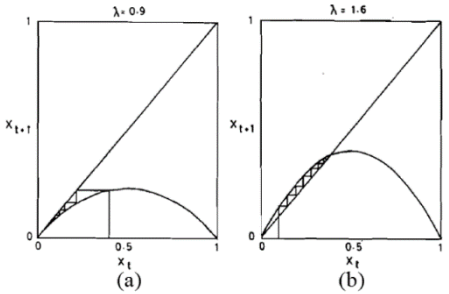

Behavior of Sand Dunes

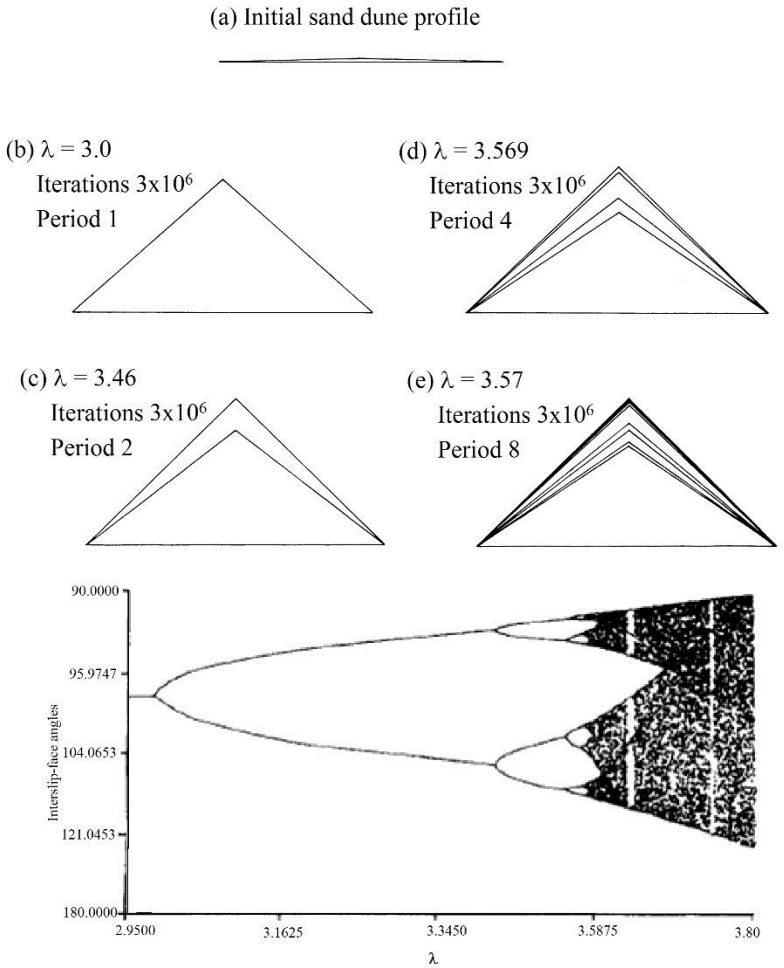

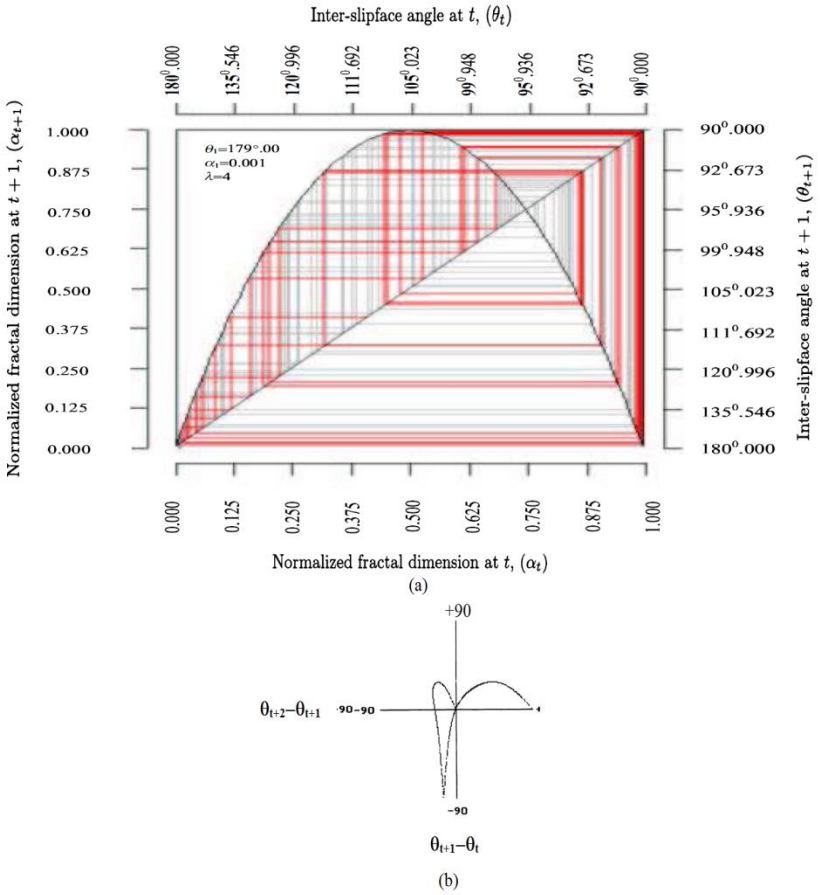

But too many questions on DATA…

- What is the noise sensitivity on the final results?
- Noise the component that does not contribute anything to the process of accurate predictions
- Noise misleads the accurate prediction process.
- How to detect the noise?
- How to make the data noise-free?
- A crude definition of ‘noise’ is the component that does not have any relationship with the main components. How to make the distinction between the noise-component and the main-component?
- Scalability of data—’Small is Beautiful”
- How to scale the data to the smallest possible such that it does not affect the results?
- More and more data is getting aded. What is its impact on the final predictions?
- How stable are the predictions made across spatial and/or temporal scales?

Open Challenge

- Can we construct system-specific attractor(s) with all these ingredients?
- Addressing such a challenge may provide rich clues and insights in our strides and struggle to make precise predictions!
- “At the end this is not a job of one person. A great team work with excellent coordination is required”.

I am grateful to the IEEE Geoscience and Remote Sensing Society (GRSS) for the Distinguished Lectureship (DL) opportunity and to the IEEE GRSS Brazil Chapter for hosting.

Key References

-B. S. Daya Sagar and Jean Serra, 2010, Preface: Spatial Information Retrieval, Analysis, Reasoning and Modelling, *International Journal of Remote Sensing*, v. 31, no. 22, p. 5747-5750.
-Georges Matheron, 1975, *Random Sets and Integral Geometry* (New York: John Wiley & Sons).
-Jean Serra, 1982, *Image Analysis and Mathematical Morphology*, Academic Press: London, p. 610.
-Pierre Soille, 2010, *Morphological Image Analysis: Principles and Applications*, Springer, p. 408.
-B. S. Daya Sagar, 2013, *Mathematical Morphology in Geomorphology and GISci*, CRC Press: Boca Raton, p. 546.

Q&A